Accepted Manuscript

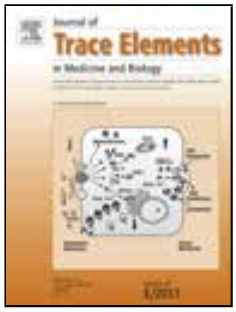

Title: Anticancer<!–<query id="Q1">Please check the presentation of the document header, and correct if necessary.</query>–> properties of sodium selenite in human glioblastoma cell cluster spheroids

Authors: Sylvie Berthier, Josiane Arnaud, Pierre Champelovier, Edwige Col, Catherine Garrel, Cécile Cottet, Jean Boutonnat, François Laporte, Patrice Faure, Florence Hazane-Puch

PII: S0946-672X(17)30156-6
DOI: http://dx.doi.org/doi:10.1016/j.jtemb.2017.04.012
Reference: JTEMB 25924

To appear in:

Received date: 23-3-2017
Accepted date: 24-4-2017

Please cite this article as: {http://dx.doi.org/

Anticancer Properties of Sodium Selenite in Human Glioblastoma Cell Cluster Spheroids

Sylvie Berthier[1], Josiane Arnaud[2,3,4], Pierre Champelovier[1], Edwige Col[1], Catherine Garrel[2], Cécile Cottet [3,4], Jean Boutonnat[1], François Laporte[2], Patrice Faure[2, 5*] and Florence Hazane-Puch[2*].

[1] Cytology Unit, Department of Anatomy and Pathologic Cytology (DACP)

[2] Hormonal and Nutritional Biochemistry Unit, Department of Biochemistry, Toxicology and Pharmacology (DBTP)

[3] University Grenoble Alpes, LBFA and BEeSy, Grenoble, France

[4] Inserm, U1055, Grenoble, France

[5] Laboratory Hypoxia and Pathology (HP2), Inserm U1042, Faculty of Medicine and Pharmacy, Domaine de la Merci, 38700 La Tronche, France.

[1, 2] from Institute of Biology and Pathology, Grenoble Alpes Hospital, CS10217, France.

*PF and FHP contributes equally to this work

Running title: Selenite anticancer properties in 3D Glioblastoma.

Corresponding author

Dr Florence Hazane-Puch

Institute of Biology and Pathology

Grenoble Alpes Hospital-DBTP-BHN

CS10217, Grenoble

France.

Tel: 0033476769316; Fax: 0033476765664;

Email: FPuch@chu-grenoble.fr

Abbreviations

3D culture: Three dimension cell culture

ABC: ATP-binding cassette

ANOVA: analysis of variance

AOBS: Acousto-Optical Beam Splitter

APMA: amino-phenyl mercuric acetate

BBB**:** blood brain barrier

BSA: bovine serum albumin

BTC: brain tumour cell

CA9: carbonic anhydrase 9

DMEM : Dulbecco's Modified Eagle Medium

DTNB: 5,5'-dithio-bis-[2-nitrobenzoic acid] or Ellman reagent

E-Cad: epithelial cadherin

ECM: extracellular matrix

EMT: epithelial to mesenchymal transition

FACS: Fluorescence-activated cell sorting

FCS: foetal calf serum

FDA: Fluorescein Diacetate

FITC: fluoresceine isothiocyanate

GAPDH: glyceraldehyde 3-phosphate deshydrogenase

GF: growth factor

GSH: glutathione

H3K9m2: dimethyl-histone-3-lysine-9

HAT: histone acetyl transferase

HDAC: histone deacetylase

HDACi: histone deacetylase inhibitor

HIF-1α: hypoxia inducible factor-1 alpha

HPRT-1 hypoxanthine phosphoribosyltransferase-1

IC50: 50% cell viability

IC50sd: 50% decrease in spheroid diameter

ICP-MS: Inductively coupled plasma mass spectrometry

IHC: immunohistochemistry

MCTS: multicellular tumor spheroid

MGMT: O(6)-methyguanine-DNA-methyltransferase

MI: mitotic index

MTP: mitochondrial trans-membrane potential

N-Cad : N-cadherin

PFA: paraformaldehyde

PI: propidium iodide

PS: penicillin-streptomycin

RT: reverse transcription

RPL27: ribosomal protein L27

RPL32: ribosomal protein L32

SDS: sodium dodecyl sulfate

Se: selenium

SeMet: seleno-L-methionine

SEPW1: Selenoprotein W1

SS: sodium selenite

TNB: 2-nitro-5-thiobenzoate

Tris-HCl: 2-Amino-2-(hydroxyméthyl)propane-1,3-diol hydrochloride

TSA: Trichostatin A

VPA: valproic acid

Graphical abstract

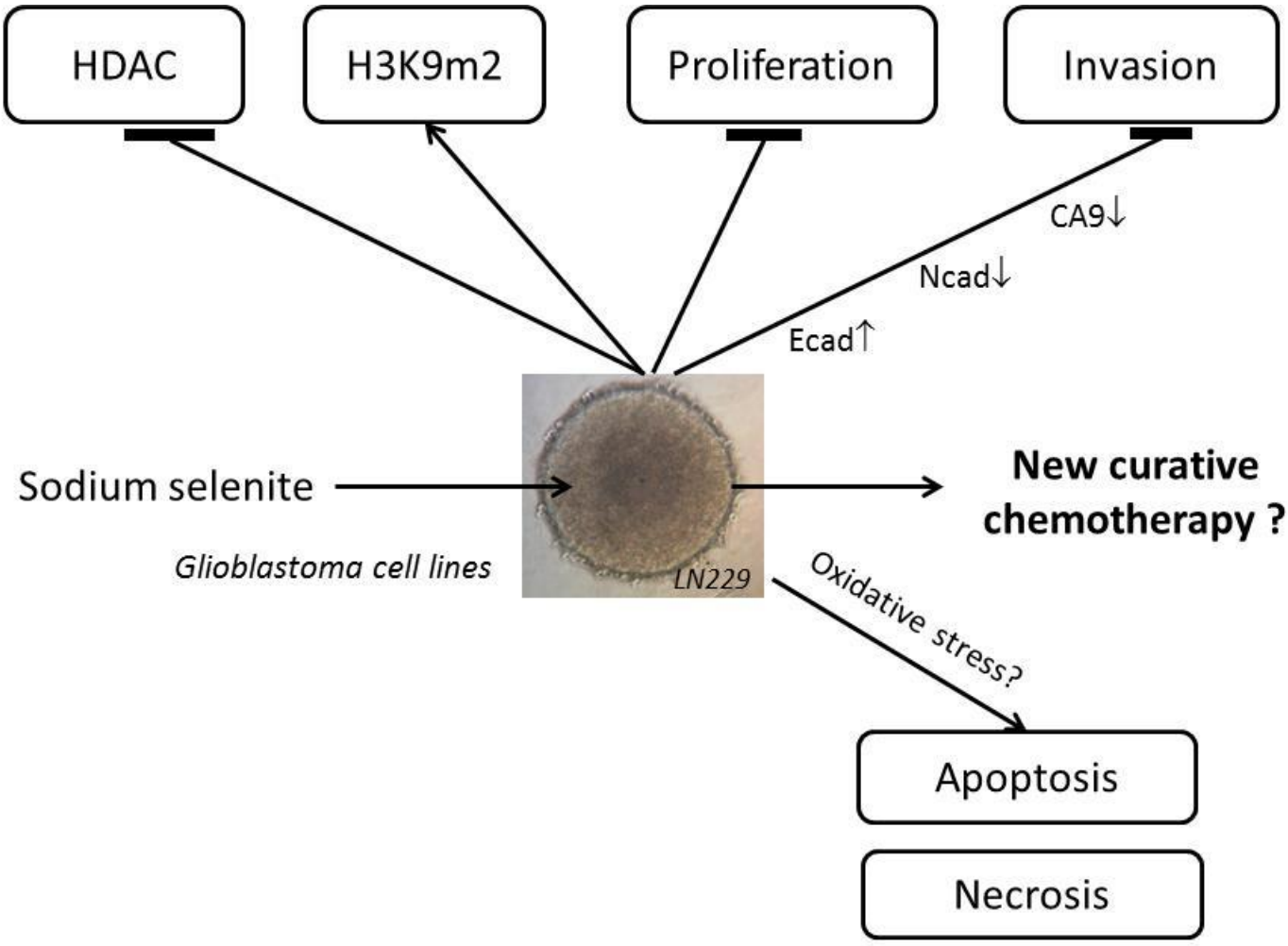

HIGHLIGHTS

Sodium selenite is more cytotoxic than temozolomide in spheroid GBM cell lines

Sodium selenite may act as an epigenetic modulator

Sodium selenite restored apoptosis in GBM cell lines cultured in 3D

Sodium selenite blocked GBM cell proliferation in S phase

Sodium selenite inhibited GBM cell migration and invasion

Abstract

Glioblastoma (GBM) is the most common type of primary tumour of the central nervous system with a poor prognosis, needing the development of new therapeutic drugs. Few studies focused on sodium selenite (SS) effects in cancer cells cultured as multicellular tumor spheroids (MCTS or 3D) closer to *in vivo* tumor.

We investigated SS anticancer effects in three human GBM cell lines cultured in 3D: LN229, U87 (O(6)-methyguanine-DNA-methyltransferase (MGMT) negative) and T98G (MGMT positive). SS absorption was evaluated and the cytotoxicity of SS and temozolomide (TMZ), the standard drug used against GBM, were compared. SS impacts on proliferation, cell death, and invasiveness were evaluated as well as epigenetic modifications by focusing on histone deacetylase (HDAC) activity and dimethyl-histone-3-lysine-9 methylation (H3K9m2), after 24h to 72h SS exposition.

SS was absorbed by spheroids and was more cytotoxic than TMZ (i.e., for LN229, the IC50 was 38 fold-more elevated for TMZ than SS, at 72h). SS induced a cell cycle arrest in the S phase and apoptosis via caspase-3. SS decreased carbonic anhydrase-9 (CA9) expression, invasion on a Matrigel matrix and modulated E- and N-Cadherin transcript expressions. SS decreased HDAC activity and modulated H3K9m2 levels.

3D model provides a relevant strategy to screen new drugs and SS is a promising drug against GBM that should now be tested in GBM animal models.

Keywords: glioblastoma human cells; spheroids; sodium selenite; anticancer drug; apoptosis; epigenetics.

Introduction

Glioblastoma represents the most common type of central nervous system primary tumour characterized by a poor prognosis with a 3-years survival rate of 16% (1). The standard treatment for GBM consists of surgery, radiotherapy and adjuvant temozolomide (TMZ) chemotherapy (2). TMZ methylates guanine and adenine which results in base mismatches at the next cell cycles and eventually strand breaks and apoptosis. However, 90% of patients are resistant to TMZ (1-3), mainly due to O(6)-methylguanine-DNA-methyltransferase (MGMT) enzyme that removes the O6-methylated guanine from DNA. Also, high expression of the enzymes of the base excision repair pathway has been shown to confer resistance to TMZ (for review (4)). In this context, the development of new therapeutic drugs is urgently needed.

Toxicity and safety of new anti-cancer drugs are mainly evaluated *in vitro* on cancer cells monolayers (2D) cultures whereas these models do not recapitulate the complexity, the physiology and the micro-environment of the tumor in the body. Indeed, tissue architecture and extracellular matrix (ECM) strongly influence tumor cell responses to micro-environmental signals. In this context, the three-dimensional (3D) culture systems or multicellular tumor spheroid (MCTS) that mimic the *in vivo* tumor tissue, are of increasing interest in cancer research (for review (5)). Spheroids are spherical cell clusters obtained by self-assembly of cells, presenting two zones: the outside proliferation zone closely reflect the *in vivo* environment of proliferating tumor cells (expressing Ki67), and the inside zone of quiescent cells showing necrotic or apoptotic cells (necrotic core) as seen in growing solid tumors (6). In tumors, quiescent cells are distant from blood vessels and expressed carbonic anhydrase 9 (CA9) due to hypoxia and to the depletion of nutrients ultimately leading to necrosis (7). By recapitulating the principal features of solid tumors, MCTS is a better model than 2D cultures, especially for drug screening purposes (6,8).

We showed that Se, an essential trace element for humans, has antagonistic effects in its SS chemical form (9): at low concentration (<1µM) SS protected skin cells against oxidative stress whereas it displayed pro-oxidant activity at higher (>5µM) concentrations (9,10). We and others reported antitumor effects of SS in brain tumor cells (11-13), by induction of apoptosis (11,13) and autophagy (14,15). Moreover, SS on 24h, was about two-fold more cytotoxic in glioma cells than in normal astrocytes (12,13). Most importantly, SS has been shown to cross the blood brain barrier (BBB) in humans (16).

Invasion and metastasis are two sequential processes of tumor cells associated to a loss of growth control implying different processes. During epithelial-to-mesenchymal transition

(EMT), the loss of E-cadherin is a critical molecular event behind cell-cell contact dissolution parallel to the induction of mesenchymal markers such as N-cadherin (17). As mesenchymal GBM are the most aggressive tumors, targeting EMT mechanisms may be of great clinical relevance in GBM (18). Moreover, hypoxia regulation via carbonic anhydrases (CA), particularly CA9, plays an important role in tumor progression and metastasis (19,20), and in tumor cell survival in the hypoxic region through the regulation of intra-cellular pH (21). In GBM, tumor cells expressed a high degree of intra-tumoral hypoxia contributing to CA9 activation through the hypoxia inducible factor-1 alpha (HIF1α) pathway (21). Moreover, CA9, absent in normal brain, is an independent poor prognostic factor in GBM (22) and may be a therapeutic target.

Glioblastoma pathogenesis may be partly due to epigenetic aberrations (23). The transcription process is regulated by chromatin packaging which is partially controlled by HDAC and histone acetyl transferases (HATs). DNA methylation and histone modifications regulated by HATs/HDACs are affected in GBM (24). As HDACs are implicated in numerous cellular activities involving transcriptional regulation, cell cycle, autophagy, apoptosis and DNA damage repair (25), HDAC inhibitors (HDACi), such as valproic acid (VPA) are nowadays the objective of cancer researches with VPA associated to reduction of cell invasiveness (26,27). Other levels of epigenic regulations are the post-translational modifications of histones (28). The methylation of H3K9 is a sign of condensed, inactive chromatin whereas methylation of H3K4 is a mark of open chromatin (29). The comprehension of epigenetic modifications induced by a drug in chromatin remodelling leading to the re-expression of tumor suppressor genes is of interest.

Herein, we show the pertinence of the 3D model mimic tumor for the evaluation of drug toxicity. We exhibit the anticancer properties of SS (compared to TMZ) in three different human glioblastoma cell lines cultured in spheroids. SS affected cell proliferation, HDAC activities, CA9 and H3K9m2 expressions, invasiveness leading to cell death.

Materials and methods

Maintenance of the cells in 2D cultures

GBM cell lines LN229, T98G and U87 were obtained from ATCC (Molsheim, France) and were maintained in RPMI 1640 medium containing 10% (v/v) fetal calf serum (FCS), penicillin 100IU/mL, streptomycin 100µg/mL, and L-glutamine (2mM) (Life Technologies, Saint Aubin, France).

3D cultures

GBM cells were cultured in 96-well tissue culture plate uncoated U-bottom (#650185; Greiner Cellstar®, Courtaboeuf, France) to allow the formation of one spheroid/well. 3000 cells/well were loaded, in the same medium than used in 2D but enriched with 0.225g/100 mL of methylcellulose (Methocel®MC, #64605, Sigma, St Quentin Fallavier, France). Each plate was centrifuged at 500g, 5 min, RT and then incubated in a humidified incubator (37°C, 5% CO_2) for 72h before the addition of SS (Sigma). The formation of spheroids was assessed by light microscope visualization. The spheroids were treated with SS for 24 to 216 hours, collected, pelleted, washed twice with PBS (#18912-014, Gibco) and adequately prepared for subsequent analysis.

Selenium absorption

Spheroids were treated with SS for 72h. Medium were kept and spheroids (two 96-well plate/condition) were subjected to five thaw-frozen cycles in sterile water. Se content was determined both in cell lysates and medium, using ICP-MS (X series II, Thermo Fisher Scientific, Bremen, Germany) as previously described (30). The percentage of Se in cell lysates versus Se added to the medium was calculated. The Se recovery was determined by adding the percentage of Se found in the medium and the lysates. Se measured in nM in cell lysates was normalized by total protein (g/L) and expressed in nmoles/g prot.

MTT assay

Cell survival was assayed by a MTT test according to the method adapted to spheroids (31). LN229, T98G and U87 were SS-treated for 24, 48h and 72h (one 96-well plate/condition) and MTT (5 mg/mL) was added to each well, for 4h, in the incubator (37°C, 5% CO_2). Each spheroid was then transferred to a new flat bottom 96-well plate and centrifuged (1000g, 5 min). The remaining medium was aspirated, 100 µL DMSO/well was added and the absorbance was recorded at 570 nm.

In parallel, a MTT assay was performed with TMZ (Temodal, MSD). TMZ was dissolved in DMSO at 10mg/mL (51.5 µM), as recommended. All cell lines were TMZ-treated at different concentrations until 1mM (194µg/mL) for 72h, or with DMSO alone (vehicle). As the IC50 was not reached, a “long term” TMZ protocol was led: spheroids were TMZ-treated for 72h at 0, 100, 200, 300, 400µM and another 72h at 0, 33.3, 66.6, 100, 133.3µM, by adding 100µL/well of fresh medium. SS and TMZ concentrations resulted IC50

were determined using GraphPad Prism via a non-linear regression (curve-fit) analysis.

Flow cytometry analysis

Spheroids were treated with SS at 2.5, 5 and 10µM (two 96-well plate/condition) at different endpoints, harvested with medium, centrifuged 3min, 360g, RT and dissociated in 100µL Accutase® with a gentle flushing for 10min, RT. Then, cells were rinsed twice with PBS.

Apoptosis and the cell-cycle were evaluated with the FITC/Annexin V Apoptosis Detection kit I and the Cycle test Plus DNA reagent kit (BD Biosciences, San Jose, CA) as recommended. The subG0G1 phase was used to determine DNA fragmentation.

For H3K9m2 analysis, 10^6 cells were fixed 30 min in paraformaldehyde (PFA) 1% on ice and then permeabilized with 0.1% Triton X100 in PBS, 30 min on ice. Cells were washed in PBS/BSA 1% twice before adding 1µL of the rabbit monoclonal antibody anti-dimethyl-H3K9 (Millipore clone, MC554, 04-768, dilution 1/200) for 45 min. The protein methylation was revealed by a (FITC)-conjugated F(ab)'2 fragment goat anti-rabbit IgG(H+L) (Beckman Coulter) for 30min on ice.

Cell fluorescence was detected with FACSCantoII (Becton Dickinson) and analysed with FACS Diva Software.

Confocal microscopy analysis

Spheroids were SS-treated for 24h and 72h, harvested, set on glass bottom Petri (35x10, Greiner, Courtaboeuf, France) and incubated with 5µM of Fluorescein Diacetate (FDA, Thermofisher Scientific, Courtaboeuf, France), 1µM Hoechst 33342 and 10mg/ml Propidium Iodide (PI) (Interchim, Montluçon, France) in an incubator (37°C, 5% CO_2) for 20 min. After staining, spheroids were mounted in the microscope incubation chamber (37°C, 5% CO_2) (POC Chamber, Pecom, Erbach, Germany). Images were collected with a Leica TCS SP2 AOBS (Acoustico Optical Beam Splitter) inverted laser scanning confocal microscope equipped with an x63 oil immersion objective (HCX PL APO 63.0x1.40). Laser fluorescence excitation and emission were 351-364/425-485 nm for Hoechst, 488/500-540nm for FDA and 543/600-650nm for PI. Confocal pinhole (Airy units) was 1 for all channels. Each experiment was performed on a randomly chosen field. 3D reconstructions were performed with Volocity software from 1µm z-step optical sections through a thickness of 20µm at the top of every spheroid. Videos are available in **SD1**.

Caspase-3 assay

Spheroids not treated or SS-treated for 72h at 5µM (two 96-well plate/condition), were harvested and lysed in 50 µL Caspase-3 lysis buffer (#K105, Fluorometric Assay, BioVision, Mountain View, CA). The protein content was determined and the caspase-3 activity was measured as previously described (32).

SS effects on GBM cell growth

Spheroids were treated with SS at 2.5, 5, 10, 20 and 30µM/well (one 96-well plate/condition). Cell growth was determined by measuring the spheroid diameter (µm) until 96h, using a graduated calibrated inverted microscope (CK2, Olympus, Japan). The corresponding IC50sd (SS concentration necessary to decrease spheroid diameter by 50%) was obtained by compiling the values in GraphPad Prism via a non-linear regression (curve-fit) analysis.

Thiols groups and glutathione measurements

Spheroids were treated with SS, 2.5 and 5µM for 24h, harvested and lysed in sterile water by five thaw-frozen cycles, to obtain cell lysates.

Protein oxidation was evaluated by measuring thiol group concentrations as previously described (10). The thiol groups were expressed as micromoles/g total proteins and in percentage of the control cells.

Glutathione (GSH) was measured in 400µL of cell lysates treated with 3.6 mL of metaphosphoric acid (#20632.0236, Prolabo). After centrifugation (4000g, 10min, 4°C), GSH was determined enzymatically in the acidic protein-free-supernatant, as previously described (33).

Spheroid migration on Matrigel coated-Petri dishes

Spheroids were prepared as described and ten were deposited on BD Matrigel™ Basement Membrane Matrix (#354248, Corning)-coated dishes. Matrigel™ was dissolved (1:32) in a serum-free medium (Dulbecco's Modified Eagle Medium (DMEM-F12 medium, #31765-027, Life Technologies), enriched with 20 ng/mL human epidermal growth factor (EGF, #130-093-825), human fibroblast growth factor-2 (FGF-2, #130-093-564), and 1X MACS NeuroBrew-21 (#130-093-566) all from Miltenyi Biotec (Bergirsch Gladbach, Germany), and supplemented with 1% penicillin-streptomycin (Life Technologies). The medium was put in excess (2mL) in 10cm-Petri dishes, placed in the incubator (1h). The

unbound Matrigel™ was removed by aspiration before spheroids deposition. Serum-free medium (10mL) was then added in each Petri-dish. SS was added in the Matrigel™ or in the medium, both at 5µM. The spheroid grow was followed until 192h. The spheroid diameter was measured using a graduated scale placed into the microscope objective and pictures were taken. Results were compared to the control. Scale bar=500µm.

Real time PCR

Spheroids were SS-treated for 24 or 72h (excepted for MGMT status) and transcript expression was evaluated by reverse transcription (RT)-q-PCR, as previously described (10) and by using the comparative threshold cycle (Ct) method (34). The primer (Life Technologies) sequences were: CA9 Forward (F)-TTT GCC AGA GTT GAC GAG GC, Reverse (R)-GCT CAT AGG CAC TGT TTT CTT CC, E-Cad: (F)-ATT TTT CCC TCG ACA CCC GAT, (R)-TCC CAG GCG TAG ACC AAG A, N-Cad: (F)-TCA GGC TGT GGA CAT AGA AAC C, (R)-GCT GTA AAC GAC TCT GGC ACT, MGMT: (F)-ACC GTT TGC GAC TTG GTA CTT (R)-GGA GCT TTA TTT CGT GCA GAC C, HPRT1: (F)-CTC ATG GAC TGA TTA TGG ACA GGA C, (R)-GCA GGT CAG CAA AGA ACT TAT AGC C, RPL27: (F)-TGA TGG CAC CTC AGA TCG C, (R)-AGA GTA CCT TGT GGG CAT TAG G and RPL32: (F)-TTA AGC GTA ACT GGC GGA AAC, (R)-GAG CGA TCT CGG CAC AGT AA (all 400nM, 60°C). The amount of target gene was normalized to housekeeping genes (HPRT1, RPL27, RPL32) and expressed relative to the control cells (not SS treated).

Immunohistochemistry of CA9

A cytoblock was performed using the Shandon Cytoblock kit (Thermo scientific), which was paraffin embedded. Sections were deparaffined and incubated with the rabbit primary polyclonal CA9 antibody (ab15086, Abcam, d1:1000) for 1h, RT. A standard three-stage indirect immunoperoxidase technic was performed on a Benchmark XT Ventana staining module using an XT UltraView DAB kit; antigen retrieving was performed with the Cell Conditioning buffer CC1 (Tris/Boric acid/EDTA pH8.0) for 30min, according to the manufacturer's instructions (Ventana, Tucson, AZ, USA). No signal amplification was required. Pictures were captured using a digital camera Canon EOS400 on an inverted microscope.

HDAC activity

Spheroids were treated for 72h with 2.5 µM and 5µM SS (two 96-well plate/condition), harvested, rinsed twice in PBS and submitted to five thaw-frozen cycles in 400µL sterile water. In parallel, SS or Trichostatin A (TSA), both at 20µM, were directly added into not treated spheroids cell lysates. Samples were kept to determine protein concentration and HDAC activity was determined in cell lysates from 50µg total protein using Fluorometric Assay (#K330, BioVision, CA) as described by the manufacturer.

BCA assay

Total protein concentration was determined using the BCA assay (Interchim, Montluçon, France) as previously described (9). The absorption at 562nm was measured using the Varioskan Flash (Thermo Fisher Scientific) associated to the SkanIt Software for the quantification.

Statistical analysis

Results are expressed as means±SD for the number of experiments indicated. All statistical analysis of data was computed using StatView® (SAS Institute, CA). The sources of variation for multiple comparisons were assessed by one-way analysis of variance ANOVA. The differences were considered statistically significant at $p<0.05$.

Results

SS is absorbed in spheroids

Firstly, we wanted to evaluate the absorption of SS by spheroids. Se uptake and recovery were established both in cell lysates and medium by ICP-MS (**Table 1**). Se was absorbed by all cell lines with a maximum of 1.23% in T98G (**Table 1A**). The percentage of Se recovery, obtained by adding nmoles of Se in the medium and in the lysates, almost reached 100% with a tendency to decrease depended on SS concentration (**Table 1A**).

The quantity of absorbed Se (nmoles/g prot) augmented with increasing concentrations of SS for T98G whereas maximal absorption was obtained with 10µM in LN229 and U87. T98G exhibited the highest quantity of Se absorbed with more than 2 and 4 times more Se absorbed than in LN229 and U87 at 10 and 15µM respectively (**Table 1B**).

SS triggered apoptosis and necrosis via DNA fragmentation and caspase-3 activation

MGMT status was verified by real time-PCR in the three cell line to estimate whether it is linked to SS and TMZ responses. As known, LN229 and U87 were MGMT negative (No Ct, real-time PCR assay) whereas T98G was positive (Ct=26.11). MTT assay showed that SS was cytotoxic depended on concentrations and duration of treatment: IC50 significantly decreased between 24 and 72h SS-treatment (**Fig.1A**) and was comparable between LN229 and U87 whereas T98G was significantly more sensitive to SS than LN229 and U87 at 48h and 72h ($p<0.05$), which is interesting as T98G is MGMT negative.

In all cell lines, TMZ was not cytotoxic until 1mM-72h (**data not shown**), then we performed a TMZ long term treatment consisted in 72h treatment followed by another 72h. TMZ was cytotoxic only in LN229 and U87 (**Fig.1B)** whereas IC50 was not reached in T98G, in accordance to its MGMT status. The TMZ IC50 values are much more important than those obtained after SS treatment at 72h (6.7µM vs 252.5µM in LN229 and 46.0µM vs 72.5µM in U87).

T98G did not tolerate the Accutase® treatment to dissociate cells from the spheroids explaining the high percentage of apoptotic cells (Q4) in the control that is why we presented only 24h T98G results (idem for cell cycle analysis).

SS slightly (but significantly) increased the DNA fragmentation in T98G at 10µM-24h and 5µM-72h in U87 and 10µM-72h in LN229 (**Fig.2B**).

SS significantly induced both necrosis and apoptosis (**Fig.1C**) in T98G and U87 at 24h and in LN229 at 72h, confirmed by confocal analysis in all cell lines **(Fig.1D)**. The 3D images and videos (**SD1**) showed that SS increased the number of dead cells (PI positive and FDA negative) depended on doses and time and was cell line dependant. Indeed, LN229 seemed more resistant as 10µM-72h of SS was required to induce cell death, whereas this process was initiated at 5µM-24h of SS in T98G and U87 **(Fig.1D)**.

Finally, the apoptotic cell death was confirmed by significant increase of caspase-3 activity in all cell lines treated by 5µM-72h of SS (**Fig.1E**).

SS decreased cell proliferation and modulated cell cycle

Cell proliferation was evaluated by using different methods (**Fig.2**).

The spheroid diameter decreased with SS treatment in a time- and dose-dependent manner (**Fig.2A**). The IC50sd values decreased significantly with time and T98G was significantly more sensitive than LN229 and U87, and were close to the IC50 obtained after the MTT assay (**Fig.1A**). The diameter decrease can be linked to proliferation deceleration, checked by cell cycle analysis.

The cell cycle analysis 24h and 72h after SS treatment at 2.5, 5 and 10µM (**Fig.2B**) showed that SS affected significantly the cell cycle at 24h at 10µM, for LN229 and U87. After 72h SS-treatment, U87 cell cycle was perturbed at 5µM whereas 10µM are required to alter the cell cycle of LN229. U87 seemed more sensitive to SS. T98G cell line were also tested but its sensitivity to Accutase compromised the results at 72h treatment. Nevertheless, in all the cell lines, the cell cycle was blocked in the S phase.

Thiols groups and glutathione measurements

In order to understand whether an oxidative stress would be responsible for SS cytotoxicity, we measured thiol groups and GSH in the spheroid cell lysates, which were not modulated in LN229 and U87 (**data not shown**) but significantly decreased in T98G. The mean±SD (percentage vs control (referred as 100%), n=3 independent experiments) of 1) thiol groups were: 54.1%±10.8 at 5µM ($p=0.002$) and 28.6%±15.2 at 10µM ($p<0.0001$) and 2) GSH were: 25.5%±14.8 at 5µM ($p=0.0007$) and 25.9%±35.2 at 10µM ($p=0.0012$), suggesting an oxidative stress.

SS altered invasion potential of GBM

Spheroids from all cell lines were able to attach and migrate on a Matrigel™ matrix (**Fig. 3**). If this process was weakly inhibited at 2.5 µM (**data not shown**), it was clear at 5µM SS in the medium. Indeed, the cell migration from the spheroid was significantly inhibited at 48h in U87, 72h in T98G and 96h in LN229 (**Fig.3A**). SS had no effect on cell detachment and migration when added into Matrigel™.

Pictures showed that cell detachment and migration patterns seemed similar between all cell lines by forming a cell ring around the spheroid (**Fig.3B**). SS in the medium reduced the spheroid diameter and inhibited cell dissemination and invasion. T98G and U87 spheroids were often detached (floating) after 168h of SS treatment.

E and N-cadherin transcript expressions

To go deeper into invasiness, two actors of EMT, E- and N-Cad transcript expressions were evaluated (**Fig.3D**). Interestingly, E-Cad was not detected at baseline in LN229, T98G and U87 but SS at 72h-10µM restored significantly E-Cad transcript expression in LN229 and U87 and as a tendency in T98G, because of high response amplitudes. N-Cad transcript was expressed in all cell lines but SS significantly decreased N-Cad only in LN229 at 72h-10µM.

SS decreased CA9 expression

SS at 5 µM-24h decreased CA9 at the transcript level (**Fig.4A**) and at the protein level at 48h (**Fig.4B**). IHC staining showed CA9 protein localisation into the spheroid inside zone and an expression more intense in T98G than LN229 and U87, confirmed by real-time PCR (Ct=26.5±0.5 in T98G vs 33.6±3.8 in LN229 ($p<0.002$) and vs 33.1±2.7 in U87 ($p<0.001$)).

SS acts as an epigenetic modulator

SS decreased HDAC activity when added 72h in the medium, significantly at 10µM in LN229 and U87 and at all studied concentrations in T98G (**Fig.5A**). When SS at 20µM was added directly into cell lysates, HDAC activity was not altered, whereas TSA (positive control) at 20µM decreased HDAC activity for about 90% (**Fig.5B**). This suggests that SS is not a specific pharmacological inhibitor and affects HDAC activity by another way.

Dimethyl H3K9 level was studied in spheroids treated 24h with SS using flow cytometry (**Fig.5C**). The distribution of H3K9m2 labelling was not homogenous as two populations appeared with SS treatment: one population less methylated (named P2) and one more methylated (named P3). Consequently, we analysed the data taking into consideration these two populations. In LN229, SS at 2.5µM decreased the percentage of methylated cells, whereas it was similar to control cells at 5 and 10µM. In U87, SS did not significantly impact the percentage of unmethylated and methylated cells but significantly increased methylation levels at 10µM-24h. In T98G, these experiments were not performed as the Accutase dissociation was deleterious.

Discussion

Glioblastomas are highly aggressive tumours showing diffuse invasiveness and vascularity. Their treatment is extremely challenging due to their resistance to current treatments and to the tumor recurrence (1). Monolayer model cultures are extensively used for new drug testing, but they did not adequately represent the tissue function with its extensive cell-cell and cell-ECM interactions, which bias drug penetration, absorption and then drug toxicity. In this context, spheroid models (3D) provide a relevant link between monolayers and animal models. Therefore, based on the pioneering work of Friedrich team (8) and our previous results which describe the effect of SS on GBM cultured in 2D (11), we hypothesized that SS would exhibit anti-cancer effects in GBM cell lines cultured in 3D, in a model we developed.

The percentage of SS absorbed was quite constant whatever its concentration in LN229 and U87, whereas it increased regularly in T98G suggesting a passive process, i.e., a simple diffusion through cell membranes. T98G absorbed significantly more SS than LN229 and U87, which may explain why SS was more cytotoxic in T98G. Globally, the fact that T98G responsiveness to SS was quite different may be partly due its MGMT positive status, also correlated to TMZ resistance (1). We hypothesize that SS activity is independent from MGMT status, which would be an added value compared to TMZ. This needs further investigations by inhibiting MGMT in T98G with O-6 benzylguanine.

Absorption and toxicity of SS may be linked. Compared to 2D, SS absorption was lower (in 2D, 72h, 2.5µM=1.3%±0.4, 0.8%±0.5 and 1.1%±0.3 in LN229, T98G and U87 respectively) and IC50 was higher (in 2D, 24h=3.8±0.3µM, 6.1±0.5µM and 4.6±0.2 in LN229, T98G and U87 respectively) (11). This suggests that SS permeation through spheroid and drug delivery process decreased in 3D, maybe due to the volume of the spheroids and to more cell-cell interactions (6), mimicking what happens in tumors. However, methylselenol, a metabolite of SS, by decreasing β1 integrin expression, altered cell-cell adhesion and induced apoptosis (35). This suggests that SS could be a valuable chemopreventive drug, or used as a potentiation agent of TMZ, to facilitate cell death.

The quantity of Se measured in both lysates and cell culture medium did not allow to recover 100% of Se added, with a negative trend between the quantity added and recovery, suggesting that SS metabolism lead to the formation of volatile Se such as methylselenol, hydrogenselenide and dimethylselenide (for review (36)). A range of volatile Se-trapping methods showed that the chemical form and the matrix influenced strongly the formation of volatile Se. Indeed, only 12% of the dosed selenium was recovered in Jurkat cells incubated with methylseninic acid (37) and we did not observe this loss of recovery neither in human fibroblasts nor in HaCaT cells suggesting a specific SS metabolism in GBM cells, particularly in T98G. Moreover, only T98G displayed a depletion of GSH and thiol group pools after SS treatment, which may be due to glutathione oxidation concomitant with selenide formation and measurable at 24h. Indeed, selenite is transformed to selenide via reduction by glutathione and by thioredoxin reductases which is subsequently methylated to methylselenol, dimethylselenide and trimethylselenonium (36). It is possible that it occurred earlier in LN229 and U87.

Consequently to its absorption, SS triggered anti-cancer effects, at least in part via epigenetic modifications, by modulating HDAC activity and H3K9m2 levels, although it is not a specific pharmacological HDACi as TSA or VPA. Both epigenetic modifications may

interferes with transcript regulation (via chromatin condensation for example (29)) which in turn can lead to growth arrest and cell death (25,26). Indeed, SS inhibited cell proliferation in all GBM cell lines parallel to an apoptosis induction via caspase-3, but also a necrotic and a DNA fragmentation processes. Autophagy process was also reported in malignant glioma cells SS-treated (12). SS also blocked all the cell lines in the S phase, whereas we observed this blockage in G2 in the same cell lines cultured in 2D (11), implying that cellular organization within the spheroids influence SS effects. The spheroid model has been characterized by homocellular cell-cell interactions, leading to the formation of a spherical cell-cluster (38), that may lead to a higher activation of PI3K/Akt pathway, implied in mediated survival signals (39). It is then possible that signaling cascades activated lead to a specific cell growth arrest. The exact function of gap junctions, described to mediate homocellular GBM interactions (40) in GBM drug resistance, need to be explored, but Westhoff *et al*., proposed that by blocking gap junction formation, diminishing cell-cell interactions, GBM cell lines are sensitized to apoptosis (41). Even H3K9m2 levels were differently modulated whether SS treatment occurred in 2D (data not shown) or in 3D, with a clear increase in 2D and more nuanced effect in 3D. It could be interesting to evaluate whether the two populations corresponded to a cell position in the cluster and to determine whether it is linked to a biological effect, such as apoptosis and expression of tumor suppressor genes. Some studies proposed that SS may activate apoptosis through ROS-mediated mitochondrial dysfunctions (12,14).

In the EMT process, the overexpression of N-cadherin lead to cell-to-cell contact loss and increased invasiveness (17), whereas the re-expression of E-Cadherin suppressed tumor cell growth and invasion (42). Our results confirmed that E-cadherin transcript was not detected in all cell lines, as reported previously in GBM (17,43). We showed that SS blocked invasion maybe through down-regulation of N-Cad and upregulation of E-Cad in all cell lines. Attacking N-Cad and CA9 may be a good anti-invasiveness strategy. Srivastava *et al.* reported that MS-275 inhibited tumor cell proliferation, angiogenesis and reverse EMT *in vivo* in a breast cancer xenograft model, by triggering cadherin shift (44).

The extensive cell-cell interactions induced a hypoxic process as shown in tumoral tissue from glioblastoma (22), confirming that spheroids mimic tumoral tissue. CA9 over-expression has been associated to tumor cell growth, survival, metastatic process and invasion, all decreased by CA9 inhibitors (45,46). Our results showed that SS inhibited CA9 transcript expression at doses (5µM-24h) that did not induce cell death, whereas at higher dose (10µM-24h), its inhibition was concomitant with the apoptotic process, in agreement

with studies demonstrating that CA9 inhibitors trigger apoptosis process through mediation of ceramide synthesis (45,47). The CA9 loss expression may also be linked to cell invasion and MMP2 and MMP9 activity inhibitions (48).

Conclusion

In conclusion, we showed that spheroids are a good model to screen new anticancer drugs (here SS) before launching animal tests. SS was able to target cell death, proliferation, migration and invasion at least partly via an epigenetic modification. SS is a good candidate to be added to the list of GBM potential drug, especially because of its ability to cross human BBB (16). Further studies in GBM rat models are now necessary to investigate the SS penetration in the brain, tumor growth and toxic-side effects.

Acknowledgements

The authors thank A.Soldini and Y.Maffren for cellular and molecular biology experiments, M.C.Bouillet and D.André for Se measurements and F.Agasse for the careful reading of the manuscript.

Funding: Grenoble Alpes University Hospital

Statement of contributions

Conception and design: SB, PC, FHP; Development of methodology: SB, JA, PC, EC, CG, CC, FHP; Acquisition of data: SB, PC, EC, CC, FHP; Analysis and interpretation of data: SB, JA, PC, CC, JB, FL, PF, FHP; Writing, review: SB, JA, PC, CC, FHP; Administrative, technical and material support: SB, JA, PC, EC, CG, CC, JB, FL, PF; Study supervision: SB, PC, FHP.

References

1. Stupp R, Hegi ME, Mason WP, van den Bent MJ, Taphoorn MJ, Janzer RC, Ludwin SK, Allgeier A, Fisher B, Belanger K, Hau P, Brandes AA, Gijtenbeek J, Marosi C, Vecht CJ, Mokhtari K, Wesseling P, Villa S, Eisenhauer E, Gorlia T, Weller M, Lacombe D, Cairncross JG, Mirimanoff RO. Effects of radiotherapy with concomitant and adjuvant temozolomide versus radiotherapy alone on survival in glioblastoma in a randomised phase III study: 5-year analysis of the EORTC-NCIC trial. The Lancet Oncology 2009;10(5):459-466.

2. Stupp R, Hegi ME, van den Bent MJ, Mason WP, Weller M, Mirimanoff RO, Cairncross JG. Changing paradigms--an update on the multidisciplinary management of malignant glioma. Oncologist 2006;11(2):165-180.
3. Weller M, Cloughesy T, Perry JR, Wick W. Standards of care for treatment of recurrent glioblastoma--are we there yet? Neuro Oncol 2013;15(1):4-27.
4. Zhang J, Stevens MF, Bradshaw TD. Temozolomide: mechanisms of action, repair and resistance. Curr Mol Pharmacol 2012;5:102-114.
5. Vinci M, Gowan S, Boxall F, Patterson L, Zimmermann M, Court W, Lomas C, Mendiola M, Hardisson D, Eccles SA. Advances in establishment and analysis of three-dimensional tumor spheroid-based functional assays for target validation and drug evaluation. BMC Biol 2012;10:29.
6. Hirschhaeuser F, Menne H, Dittfeld C, West J, Mueller-Klieser W, Kunz-Schughart LA. Multicellular tumor spheroids: an underestimated tool is catching up again. J Biotechnol 2010;148(1):3-15.
7. Mehta G, Hsiao AY, Ingram M, Luker GD, Takayama S. Opportunities and challenges for use of tumor spheroids as models to test drug delivery and efficacy. J Control Release 2012;164(2):192-204.
8. Friedrich J, Seidel C, Ebner R, Kunz-Schughart LA. Spheroid-based drug screen: considerations and practical approach. Nat Protoc 2009;4(3):309-324.
9. Hazane-Puch F, Champelovier P, Arnaud J, Garrel C, Ballester B, Faure P, Laporte F. Long-term selenium supplementation in HaCaT cells: importance of chemical form for antagonist (protective versus toxic) activities. Biological trace element research 2013;154(2):288-298.
10. Hazane-Puch F, Champelovier P, Arnaud J, Trocme C, Garrel C, Faure P, Laporte F. Six-day selenium supplementation led to either UVA-photoprotection or toxic effects in human fibroblasts depending on the chemical form and dose of Se. Metallomics 2014;6(9):1683-1692.
11. Hazane-Puch F, Arnaud J, Trocme C, Faure P, Laporte F, Champelovier P. Sodium Selenite Decreased HDAC Activity, Cell Proliferation and Induced Apoptosis in Three Human Glioblastoma Cells. Anti-cancer agents in medicinal chemistry 2016;16(4):490-500.
12. Kim EH, Sohn S, Kwon HJ, Kim SU, Kim MJ, Lee SJ, Choi KS. Sodium selenite induces superoxide-mediated mitochondrial damage and subsequent autophagic cell death in malignant glioma cells. Cancer Res 2007;67(13):6314-6324.
13. Rooprai HK, Kyriazis I, Nuttall RK, Edwards DR, Zicha D, Aubyn D, Davies D, Gullan R, Pilkington GJ. Inhibition of invasion and induction of apoptosis by selenium in human malignant brain tumour cells in vitro. Int J Oncol 2007;30(5):1263-1271.
14. Park SH, Kim JH, Chi GY, Kim GY, Chang YC, Moon SK, Nam SW, Kim WJ, Yoo YH, Choi YH. Induction of apoptosis and autophagy by sodium selenite in A549 human lung carcinoma cells through generation of reactive oxygen species. Toxicol Lett 2012;212(3):252-261.
15. Chen XJ, Duan FD, Zhang HH, Xiong Y, Wang J. Sodium selenite-induced apoptosis mediated by ROS attack in human osteosarcoma U2OS cells. Biol Trace Elem Res 2012;145(1):1-9.
16. Cavalieri RR, Scott KG, Sairenji E. Selenite (75Se) as a tumor-localizing agent in man. Journal of nuclear medicine : official publication, Society of Nuclear Medicine 1966;7(3):197-208.
17. Kahlert UD, Nikkhah G, Maciaczyk J. Epithelial-to-mesenchymal(-like) transition as a relevant molecular event in malignant gliomas. Cancer Lett 2013;331(2):131-138.

18. Carro MS, Lim WK, Alvarez MJ, Bollo RJ, Zhao X, Snyder EY, Sulman EP, Anne SL, Doetsch F, Colman H, Lasorella A, Aldape K, Califano A, Iavarone A. The transcriptional network for mesenchymal transformation of brain tumours. Nature 2010;463(7279):318-325.
19. Brahimi-Horn MC, Chiche J, Pouyssegur J. Hypoxia and cancer. J Mol Med (Berl) 2007;85(12):1301-1307.
20. Chaudary N, Hill RP. Hypoxia and metastasis. Clin Cancer Res 2007;13(7):1947-1949.
21. De Simone G, Supuran CT. Carbonic anhydrase IX: Biochemical and crystallographic characterization of a novel antitumor target. Biochim Biophys Acta 2010;1804(2):404-409.
22. Proescholdt MA, Merrill MJ, Stoerr EM, Lohmeier A, Pohl F, Brawanski A. Function of carbonic anhydrase IX in glioblastoma multiforme. Neuro Oncol 2012;14(11):1357-1366.
23. Nagarajan RP, Costello JF. Molecular epigenetics and genetics in neuro-oncology. Neurotherapeutics 2009;6(3):436-446.
24. Lucio-Eterovic AK, Cortez MA, Valera ET, Motta FJ, Queiroz RG, Machado HR, Carlotti CG, Jr., Neder L, Scrideli CA, Tone LG. Differential expression of 12 histone deacetylase (HDAC) genes in astrocytomas and normal brain tissue: class II and IV are hypoexpressed in glioblastomas. BMC Cancer 2008;8:243.
25. Xu WS, Parmigiani RB, Marks PA. Histone deacetylase inhibitors: molecular mechanisms of action. Oncogene 2007;26(37):5541-5552.
26. Bezecny P. Histone deacetylase inhibitors in glioblastoma: pre-clinical and clinical experience. Med Oncol 2014;31(6):985.
27. Papi A, Ferreri AM, Rocchi P, Guerra F, Orlandi M. Epigenetic modifiers as anticancer drugs: effectiveness of valproic acid in neural crest-derived tumor cells. Anticancer Res 2010;30(2):535-540.
28. Nakayama J, Rice JC, Strahl BD, Allis CD, Grewal SI. Role of histone H3 lysine 9 methylation in epigenetic control of heterochromatin assembly. Science 2001;292(5514):110-113.
29. Peters AH, Mermoud JE, O'Carroll D, Pagani M, Schweizer D, Brockdorff N, Jenuwein T. Histone H3 lysine 9 methylation is an epigenetic imprint of facultative heterochromatin. Nature genetics 2002;30(1):77-80.
30. Rousset F, Hazane-Puch F, Pinosa C, Nguyen MV, Grange L, Soldini A, Rubens-Duval B, Dupuy C, Morel F, Lardy B. IL-1beta mediates MMP secretion and IL-1beta neosynthesis via upregulation of p22(phox) and NOX4 activity in human articular chondrocytes. Osteoarthritis and cartilage / OARS, Osteoarthritis Research Society 2015;23(11):1972-1980.
31. Ho WY, Yeap SK, Ho CL, Rahim RA, Alitheen NB. Development of multicellular tumor spheroid (MCTS) culture from breast cancer cell and a high throughput screening method using the MTT assay. PLoS One 2012;7(9):e44640.
32. Champelovier P, Mininno M, Duchamp E, Nicolle E, Curri V, Boumendjel A, Boutonnat J. Cytotoxicity of chalcone derivatives towards glioblastoma. Anticancer Res 2011;31(10):3213-3218.
33. Akerboom TP, Sies H. Assay of glutathione, glutathione disulfide, and glutathione mixed disulfides in biological samples. Methods in enzymology 1981;77:373-382.
34. Giulietti A, Overbergh L, Valckx D, Decallonne B, Bouillon R, Mathieu C. An overview of real-time quantitative PCR: applications to quantify cytokine gene expression. Methods 2001;25(4):386-401.

35. Kim A, Oh JH, Park JM, Chung AS. Methylselenol generated from selenomethionine by methioninase downregulates integrin expression and induces caspase-mediated apoptosis of B16F10 melanoma cells. J Cell Physiol 2007;212(2):386-400.
36. Gammelgaard B, Gabel-Jensen C, Sturup S, Hansen HR. Complementary use of molecular and element-specific mass spectrometry for identification of selenium compounds related to human selenium metabolism. Anal Bioanal Chem 2008;390(7):1691-1706.
37. Gabel-Jensen C, Lunoe K, Gammelgaard B. Formation of methylselenol, dimethylselenide and dimethyldiselenide in in vitro metabolism models determined by headspace GC-MS. Metallomics 2010;2(2):167-173.
38. Hazlehurst LA, Landowski TH, Dalton WS. Role of the tumor microenvironment in mediating de novo resistance to drugs and physiological mediators of cell death. Oncogene 2003;22(47):7396-7402.
39. Frame MC. Newest findings on the oldest oncogene; how activated src does it. J Cell Sci 2004 1(117):989-998.
40. Oliveira R, Christov C, Guillamo JS, de Boüard S, Palfi S, Venance L, Tardy M, Peschanski M. Contribution of gap junctional communication between tumor cells and astroglia to the invasion of the brain parenchyma by human glioblastomas. BMC Cell Biol 2005;16(6):1-7.
41. Westhoff MA, Zhou S, Bachem MG, Debatin KM, Fulda S. Identification of a novel switch in the dominant forms of cell adhesion-mediated drug resistance in glioblastoma cells. Oncogene 2008;27(39):5169-5181.
42. Soto E, Yanagisawa M, Marlow LA, Copland JA, Perez EA, Anastasiadis PZ. p120 catenin induces opposing effects on tumor cell growth depending on E-cadherin expression. The Journal of cell biology 2008;183(4):737-749.
43. Lewis-Tuffin LJ, Rodriguez F, Giannini C, Scheithauer B, Necela BM, Sarkaria JN, Anastasiadis PZ. Misregulated E-cadherin expression associated with an aggressive brain tumor phenotype. PLoS One 2010;5(10):e13665.
44. Srivastava RK, Kurzrock R, Shankar S. MS-275 sensitizes TRAIL-resistant breast cancer cells, inhibits angiogenesis and metastasis, and reverses epithelial-mesenchymal transition in vivo. Molecular cancer therapeutics 2010;9(12):3254-3266.
45. Cianchi F, Vinci MC, Supuran CT, Peruzzi B, De Giuli P, Fasolis G, Perigli G, Pastorekova S, Papucci L, Pini A, Masini E, Puccetti L. Selective inhibition of carbonic anhydrase IX decreases cell proliferation and induces ceramide-mediated apoptosis in human cancer cells. J Pharmacol Exp Ther 2010;334(3):710-719.
46. Lou Y, McDonald PC, Oloumi A, Chia S, Ostlund C, Ahmadi A, Kyle A, Auf dem Keller U, Leung S, Huntsman D, Clarke B, Sutherland BW, Waterhouse D, Bally M, Roskelley C, Overall CM, Minchinton A, Pacchiano F, Carta F, Scozzafava A, Touisni N, Winum JY, Supuran CT, Dedhar S. Targeting tumor hypoxia: suppression of breast tumor growth and metastasis by novel carbonic anhydrase IX inhibitors. Cancer Res 2011;71(9):3364-3376.
47. Swietach P, Patiar S, Supuran CT, Harris AL, Vaughan-Jones RD. The role of carbonic anhydrase 9 in regulating extracellular and intracellular ph in three-dimensional tumor cell growths. J Biol Chem 2009;284(30):20299-20310.
48. Radvak P, Repic M, Svastova E, Takacova M, Csaderova L, Strnad H, Pastorek J, Pastorekova S, Kopacek J. Suppression of carbonic anhydrase IX leads to aberrant focal adhesion and decreased invasion of tumor cells. Oncol Rep 2013;29(3):1147-1153.

Table

Table 1. Sodium selenite absorption

LN229, T98G and U87 cells were cultured in 3D for 72h before the addition of increasing doses of sodium selenite for 72h. Medium and cell were harvested and cells were lysed by repeated thaw-frozen cycles. Selenium was determined in cell lysates and medium using ICP-MS. Results are expressed in percentage of Se measured in each fraction, compared to Se added (A) and in nmoles of Se/g prot found in the cell lysates (B). Results are mean±SD of four independent experiments.

A.

	Se measured in percentage		
	Lysate	Medium	Total
Sodium selenite (µM)	**LN229**		
2.5	0.11 ± 0.06	94.2 ± 15.50	94.32 ± 15.51
5	0.12 ± 0.06	97.99 ± 11.44	98.11 ± 11.47
10	0.14 ± 0.05	84.66 ± 18.72	84.79 ± 18.69
15	0.14 ± 0.09	91.71 ± 10.89	91.85 ± 10.84
20	0.11 ± 0.04	76.68 ± 9.58	76.79 ± 9.62
Sodium selenite (µM)	**T98G**		
2.5	0.14 ± 0.12	89.00 ± 18.50	89.14 ± 18.61
5	0.30 ± 0.20	92.09 ± 12.74	92.39 ± 12.9
10	0.85 ± 0.24	69.855 ± 10.61	70.70 ± 10.8
15	1.23 ± 0.14	78.7 ± 5.99	79.93 ± 6.12
20	1.00 ± 0.12	78.4 ± 0.07	79.40 ± 0.19
Sodium selenite (µM)	**U87**		
2.5	0.18 ± 0.03	98.75 ± 20.24	98.92 ± 20.27
5	0.14 ± 0.06	94.88 ± 8.58	95.02 ± 8.6
10	0.23 ± 0.08	81.26 ± 15.03	81.49 ± 14.95
15	0.21 ± 0.12	83.02 ± 12.6	83.23 ± 12.67
20	0.17 ± 0.05	77.2 ± 11.36	77.44 ± 11.40

B.

	Se measured in nmoles/g prot		
Sodium selenite (µM)	**LN229**	**T98G**	**U87**
2.5	192.58 ± 33.01	565.28 ± 84.46	259.27 ± 64.93
5	1392.09 ± 1049.08	2142.45 ± 76.67	585.65 ± 259.24
10	6562.42 ± 6250.73	11274.35 ± 5024.59	5372.36 ± 733.73
15	7577.39 ± 4766.98	32231.82 ± 10703.03	5018.33 ± 3072.71
20	4794.64 ± 2338.56	43410.00 ± 20209.11	8338.21 ± 3332.63

Figure legends

Figure 1. Cell death process characterization.

LN229, T98G and U87 GBM cell lines were seeded in 96-well plate 72h before the addition of SS, to form spheroids.

A MTT assay was performed after

A. 24h, 48h and 72h SS

B. 72h TMZ treatment and then fresh medium was added for another 72h of treatment.

To avoid overloading MTT graphs, statistical items were informed when the first statistical significance was reached and for the last concentration studied. Results are means ±SD of three independent experiments, with *p<0.05, **p<0.005, $^{\$}$p<0.0001 versus the control (untreated cells). A recapitulative table presents IC50 for each cell line SS (significance given versus 24h SS-treatment) or TMZ-treated.

C. Effects of SS on cell death triggered in GBM cell lines cultured in spheroids were studied using flow cytometry, with FITC and PI staining. LN229, T98G and U87 spheroids were treated for 24h, 48h and 72h with 2.5, 5 and 10µM of SS before dissociation with Accutase. Cells in Q3 are considered as viable cells, in Q1 as necrotic cells, in Q4 as apoptotic cells and in Q2 as both apoptotic and necrotic. Results are mean ±SD of cell percentage in each phase.

D. Confocal analysis of SS-triggered cell death in spheroids. Spheroids were SS-treated for 24h, 48h and 72h, harvested and set on glass bottom Petri incubated with FDA (green signal), Hoechst 33342 (blue signal) and PI (red signal) at 37°C in a 5% CO_2 incubator. After staining, spheroids were installed on the microscope incubation chamber with controlled atmosphere. Images were collected with a Leica TCS SP2 AOBS inverted laser scanning confocal microscope equipped with an x63 oil immersion objective. Each experiment was performed on a randomly chosen field and the images are representative of two or three-independent experiments. 3D reconstructions were performed with Volocity software from 1 µm z-step optical sections through a thickness about 20µm at the top of every spheroid. Scale bar 24µm.

E. Caspase-3 activity was determined after 72h SS treatment at 5µM. Spheroids were washed twice in PBS 1X and the lysates were then used to determine caspase-3 activity using fluorometric assay kit (BioVision) as described by the manufacturer.

Results, expressed in percentage versus the control (not treated), are mean±SD of three independent experiments with *p<0.05, **p<0.005, $p<0.0001 versus the control (not treated cells).

Figure 2. Effect of sodium selenite on LN229, T98G and U87 proliferation and cell cycle.
Cells were cultured in specific 96 well plates (3000 cells/well) and were treated with SS.
A. The diameter of the spheroids was measured at different times (24, 48, 72 and 96h) after the addition of SS at increasing doses (0, 2.5, 5, 10, 20 and 30 µM). Results are representative of one out of four independent experiments.
IC50sd (SS concentration necessary to decrease the spheroid diameter by 50%, µM) indicated in the associated table are mean±SD of four independent experiments with $^{\$}p<0.0001$ vs 24h.
B. Effects of sodium selenite on the cell cycle. Spheroids were prepared as described in the material and method section (3000 cells/well), cultured for 72h before the addition of SS. After 24h and 72h of SS treatment, spheroids were harvested, washed twice in PBS 1X then used for cell cycle determination by flow cytometry. Data expressed in percentage of positive cells, are mean±SD of three independent experiments and *p value* are indicated when significant versus control.

Figure 3. Anti invasiness properties of sodium selenite
A. Detachment and migration of cells from spheroids were followed after deposition of spheroids on Matrigel coated Petri-dishes. The size of spheroids was measured until 192h after the deposit.
Results are mean diameter (µm) ±SD of three independent experiments, with $^{*}p<0.05$, $^{**}p<0.005$ vs control at 24h.
B. Pictures (X4) were taken after each measurement and are illustrative of three independent experiments. Scale bar =500µm.
C. E-cadherin and N-cadherin transcript expressions were evaluated by RT-q-PCR. LN229, T98G and U87 in 3D were treated 72h with SS. Results are mean ±SD of three independent experiments, with $^{t}p=0.07$, $^{*}p<0.05$, $^{**}p<0.005$ vs control at 24h.

Figure 4. Sodium selenite decreased CA9 expression.
CA9 expression was evaluated both
A. At the transcriptional level (real time PCR), 24h after SS treatment. Results are mean±SD of four independent experiments, expressed by fold change vs the control (not treated) with $^{***}p<0.0005$ and $^{\$}p<0.001$ vs control.
B. At the protein level, by immunohistochemistry. Pictures were performed at a magnification X400 and were representative of three independent experiments.

Figure 5. Sodium selenite is an epigenetic modulator

HDAC activity was evaluated by using a fluorometric method in

A. lysates from LN229, T98G and U87 cells cultivated in 3D for 72h and treated 72h with SS at 2.5, 5µM and 10µM. Results expressed in Relative Fluorescence Units/µg prot (% vs control) are mean±SD of three independent experiments with *$p<0.05$ and **$p<0.005$ versus the control (not treated cells).

B. TSA or SS (both at 20µM) were directly added into the lysates and HDAC activity was determined.

Results expressed in Relative Fluorescence Units/µg prot (% vs control) are mean±SD of three independent experiments with $^{\$}p<0.0001$ versus the control (not treated cells).

C. Dimethyl H3K9 level was evaluated in LN229 and U87 cultivated in 3D. Spheroids were prepared as described, treated 24h with SS and dissociated with Accutase to be analyzed by flow cytometry. Left histograms represent the percentage of labelled cells versus non labelled cells and right histogram the mean fluorescence of labelled cells in P3. Results are mean±SD of three independent experiments with *$p<0.05$ and **$p<0.005$ versus the control (not treated cells).

Figure 1. Cell death process characterization.

LN229, T98G and U87 GBM cell lines were seeded in 96-well plate 72h before the addition of SS, to form spheroids.

A MTT assay was performed after **A.** 24h, 48h and 72h SS **B.** 72h TMZ treatment, and then fresh medium was added for another 72h of treatment.

To avoid overloading MTT graphs, statistical items were informed when the first statistical significance was reached and for the last concentration studied. Results are means ±SD of three independent experiments, with *p<0.05, **p<0.005, $^{\$}$p<0.0001 versus the control (untreated cells). A recapitulative table presents IC50 for each cell line SS (significance given versus 24h SS-treatment) or TMZ-treated.

Fig. 1A

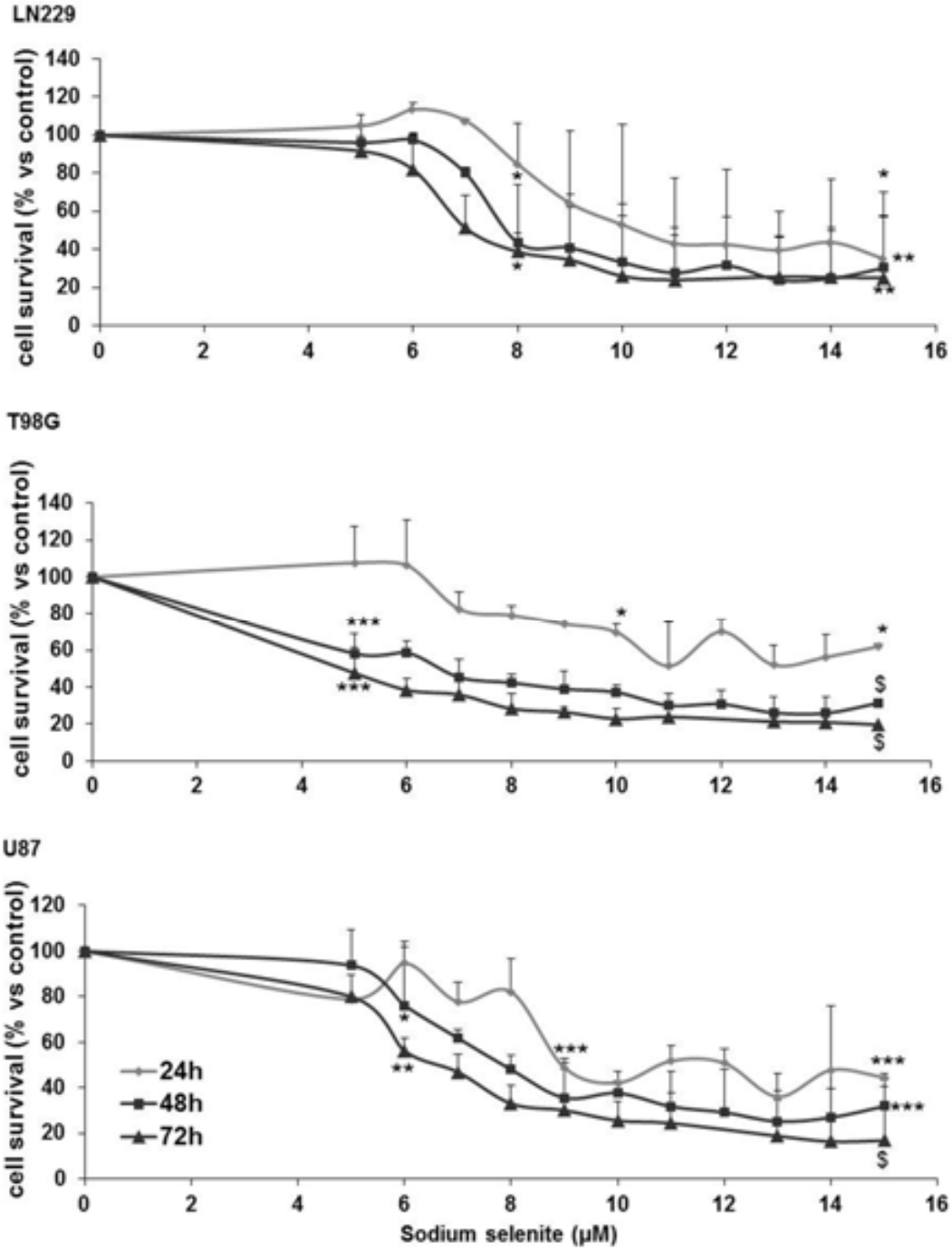

IC50 (µM)	24h	48h	72h
LN229	13.7±1.1	7.1±0.3*	6.7±0.5**
T98G	17.9±2.7	4.6±0.4$^{\$}$	4.6±0.5$^{\$}$
U87	12.1±0.6	7.0±0.3**	6.0±0.2$^{\$}$

Fig. 1B

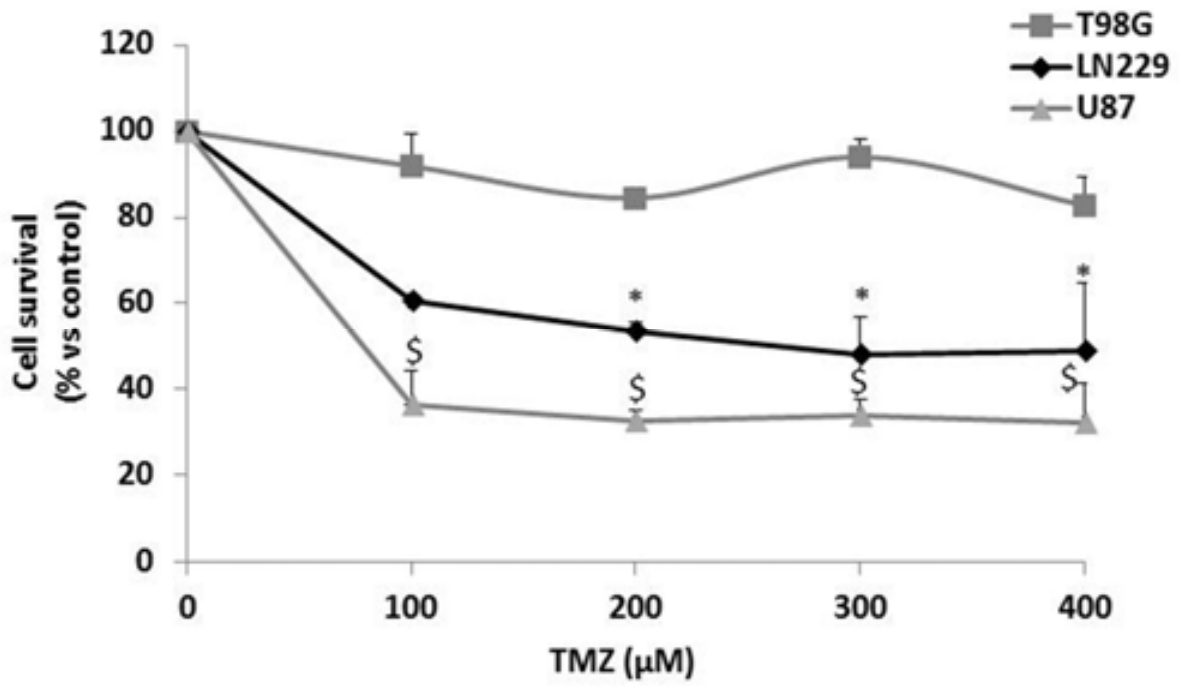

	LN229	T98G	U87
IC50 (µM)	252.5±67.5	Not reached	72.5±10.6

Fig. 1C

Effects of SS on cell death triggered in GBM cell lines cultured in spheroids were studied using flow cytometry, with FITC and PI staining. LN229, T98G and U87 spheroids were treated for 24h, 48h and 72h with 2.5, 5 and 10µM of SS before dissociation with Accutase. Cells in Q3 are considered as viable cells, in Q1 as necrotic cells, in Q4 as apoptotic cells and in Q2 as both apoptotic and necrotic. Results are mean ±SD of cell percentage in each phase.

24h

LN229

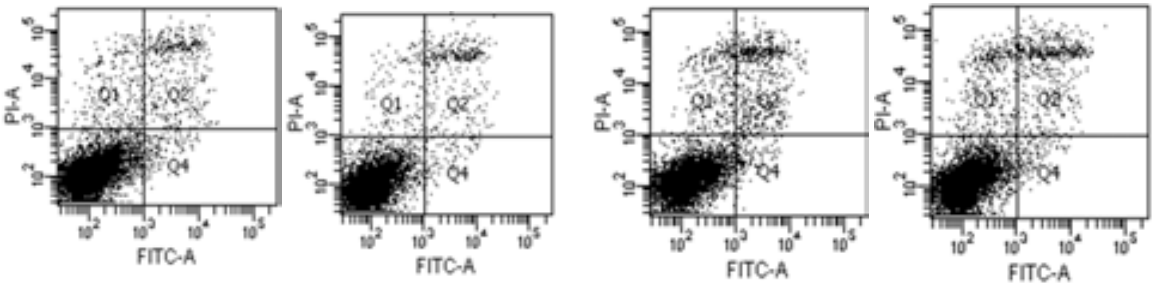

	Control	Se 2.5µM	Se 5µM	Se 10µM
Q1 IP+FITC-	3.3±0.5	5.3±3.3	5.8±3.6	6.9±3.5
Q2 IP+FITC+	9.0±1.9	5.5±0.8	5.9±0.7	9.0±2.1
Q3 IP-FITC-	85.5±2.5	87.4±2.8	86.3±2.9	82.6±2.7
Q4 IP-FITC+	2.2±0.4	1.7±0.7	1.9±0.7	1.5±0.4

U87

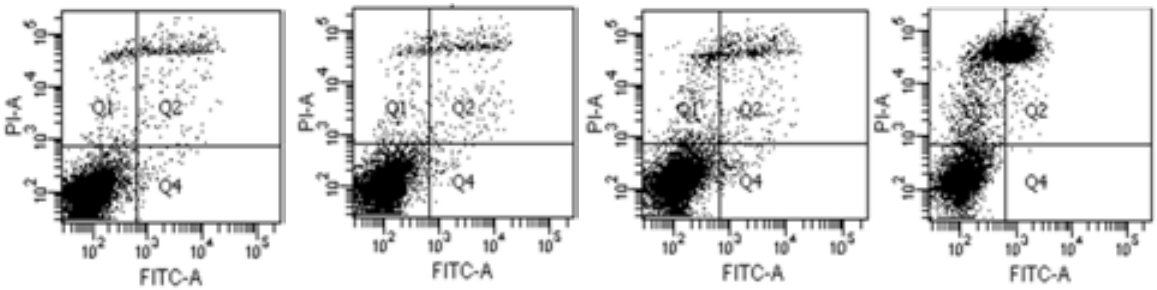

Q1 IP+FITC-	4.4±2.2	3.8±1.3	9.3±4.4	19.6±4.9 *p=0.02*
Q2 IP+FITC+	3.9±0.4	4.0±0.7	11.6±3.4	27.4±6.0 *p=0.02*
Q3 IP-FITC-	91.2±1.8	90.3±1.6	75.9±6.5	52.3±2.8 *p<0.0001*
Q4 IP-FITC+	1.2±0.3	1.8±1.1	3.1±1.6	0.6±0.6

T98G

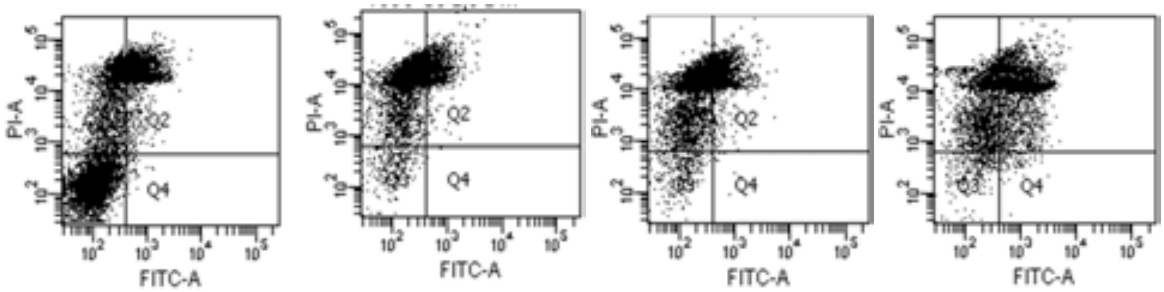

Q1 IP+FITC-	26.4±1.9	57.8±5.4 *p=0.04*	45.6±14.7	28.5±8.9
Q2 IP+FITC+	33.7±12.0	28.7±1.3	48.0±16.7	59.7±9.7
Q3 IP-FITC-	39.4±13.0	13.2±4.9 *p=0.036*	7.4±3.7 *p=0.02*	7.7±3.3 *p=0.02*
Q4 IP-FITC+	0.6±0.0	0.3±0.1	0.9±0.6	4.1±2.1

Fig. 1C (followed…)

72h	Control	Se 2.5µM	Se 5µM	Se 10µM
LN229	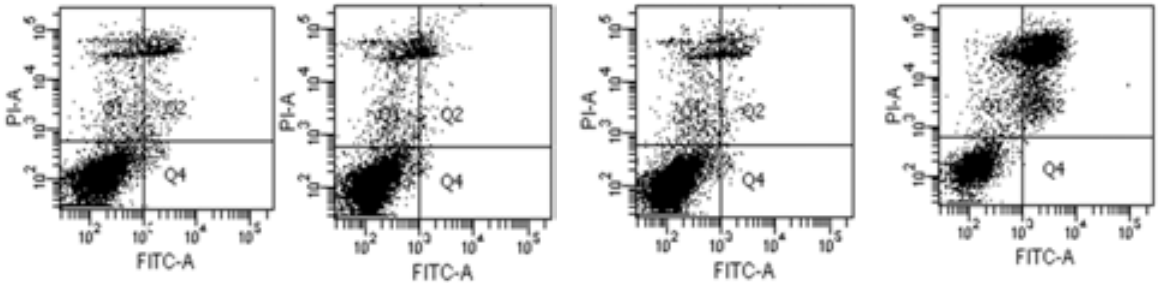			
Q1 IP+FITC-	12.2±6.5	12.2±6.3	11.3±6.1	10.5±3.7
Q2 IP+FITC+	6.9±3.3	5.8±3.0	8.5±5.8	40.6±7.0 *p=0.02*
Q3 IP-FITC-	77.5±2.5	80.9±2.8	78.7±3.4	48.0±9.9 *p=0.01*
Q4 IP-FITC+	3.3±2.5	1.0±0.7	1.4±1.1	0.9±0.6
U87	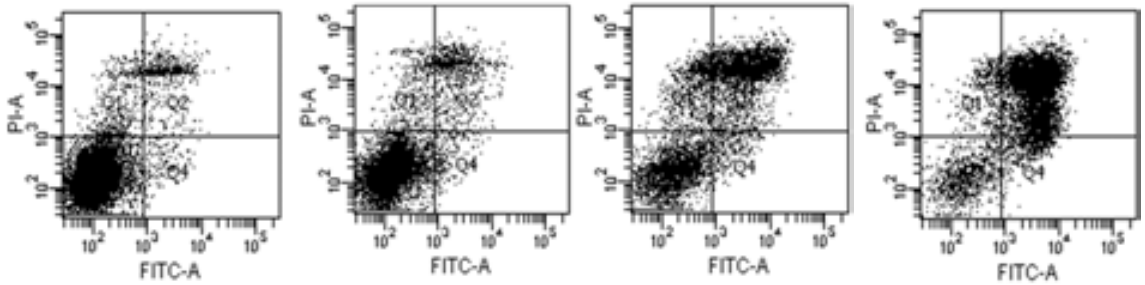			
Q1 IP+FITC-	11.6±6.5	8.3±3.2	24.5±14.0	16.2±10.9
Q2 IP+FITC+	6.6±0.1	8.8±2.4	31.5±14.3 *p=0.02*	67.3±7.8 *p=0,0002*
Q3 IP-FITC-	80.2±6.1	81.0±0.2	41.9±2.3 *p<0.0001*	12.8±0.6 *p<0.0001*
Q4 IP-FITC+	1.0±0.9	2.0±1.0	2.3±2.0	2.6±2.4

Fig. 1D

Confocal analysis of SS-triggered cell death in spheroids. Spheroids were SS-treated for 24h, 48h and 72h, harvested and set on glass bottom Petri incubated with FDA (green signal), Hoechst 33342 (blue signal) and PI (red signal) at 37°C in a 5% CO_2 incubator. After staining, spheroids were installed on the microscope incubation chamber with controlled atmosphere. Images were collected with a Leica TCS SP2 AOBS inverted laser scanning confocal microscope equipped with an x63 oil immersion objective. Each experiment was performed on a randomly chosen field and the images are representative of two or three-independent experiments. 3D reconstructions were performed with Volocity software from 1 µm z-step optical sections through a thickness about 20µm at the top of every spheroid. Scale bar 24µm.

Fig. 1D

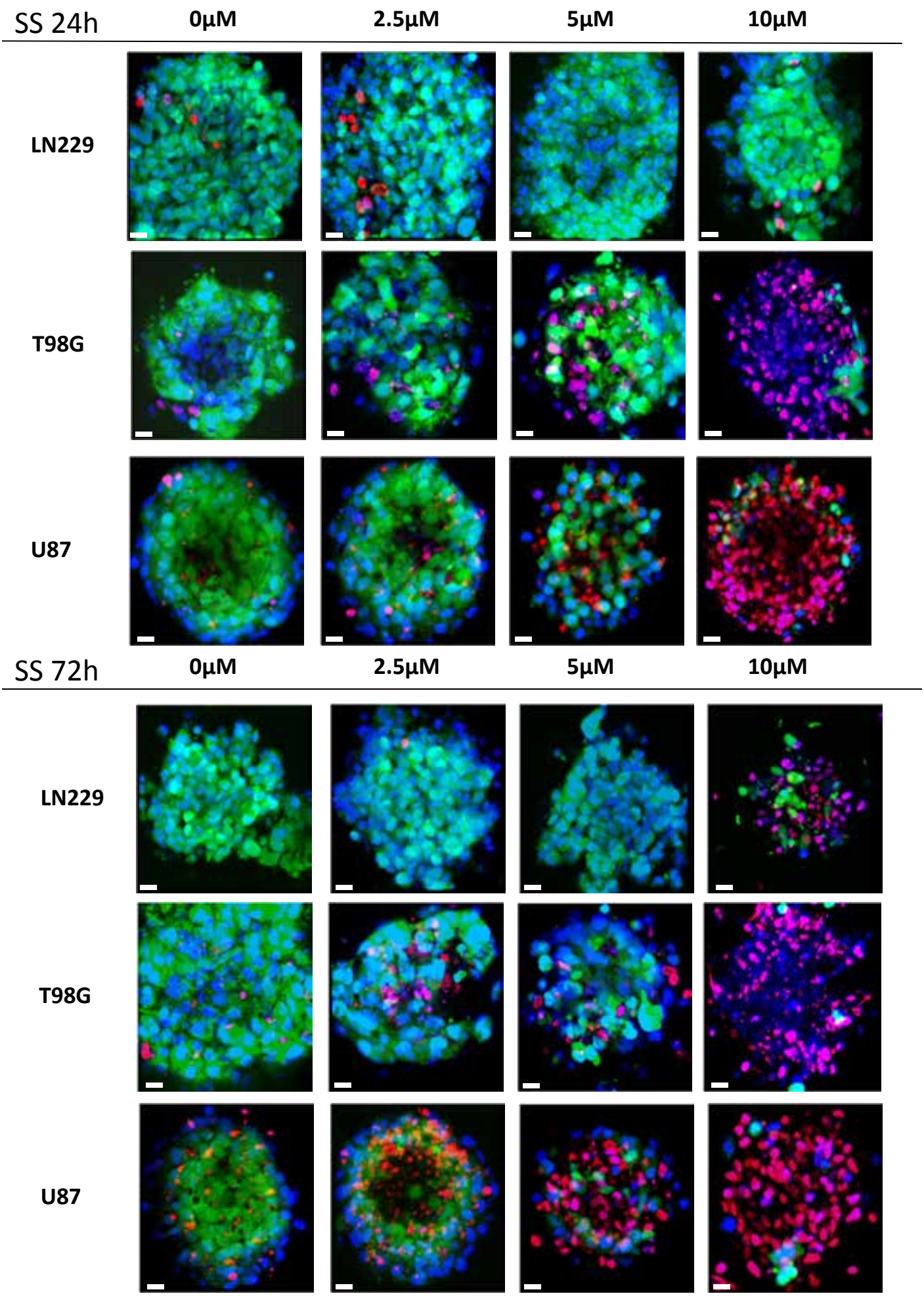

Fig. 1E

Caspase-3 activity was determined after 72h SS treatment at 5µM. Spheroids were washed twice in PBS 1X and the lysates were then used to determine caspase-3 activity using fluorometric assay kit (BioVision) as described by the manufacturer.

Results, expressed in percentage *versus* the control (not treated), are mean±SD of three independent experiments with *p<0.05, **p<0.005, $^{\$}$p<0.0001 versus the control (not treated cells).

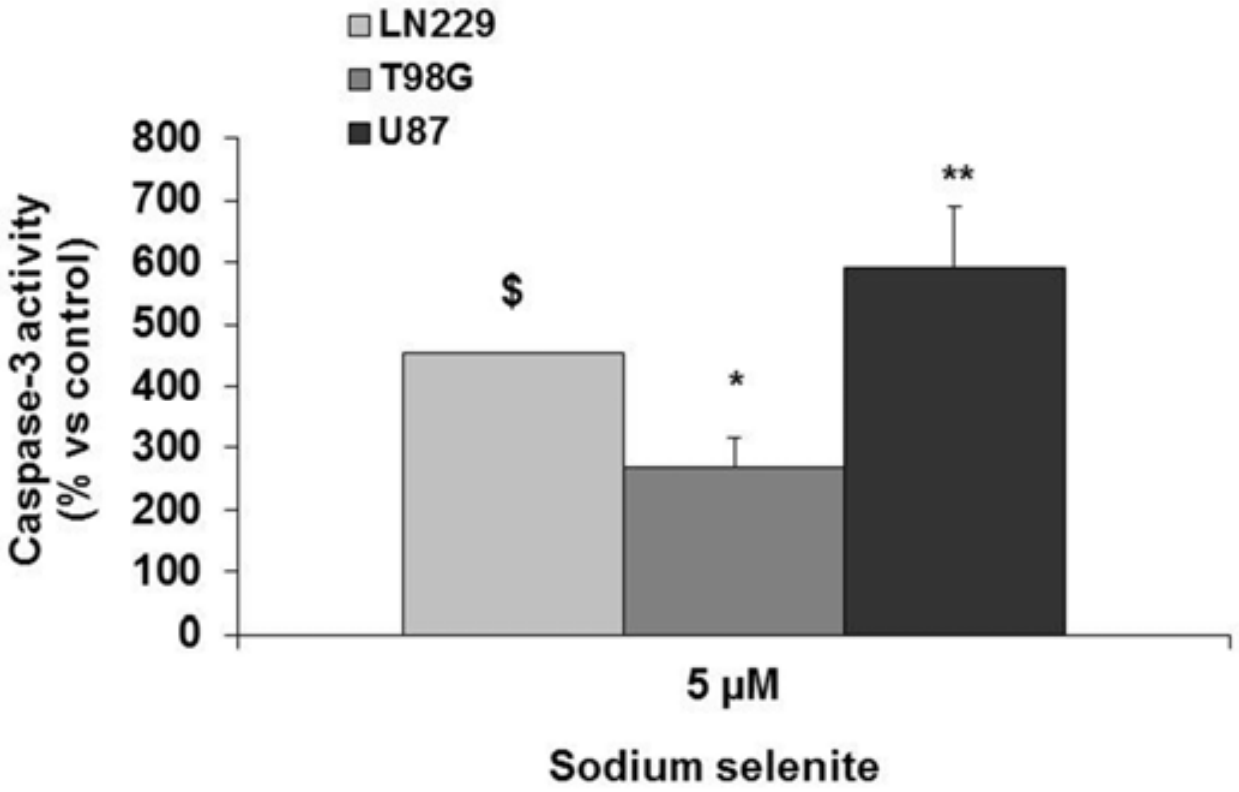

Figure 2. Effect of sodium selenite on LN229, T98G and U87 proliferation and cell cycle.
Cells were cultured in specific 96 well plates (3000 cells/well) and were treated with SS.

Fig. 2A

The diameter of the spheroids was measured at different times (24, 48, 72 and 96h) after the addition of SS at increasing doses (0, 2.5, 5, 10, 20 and 30 µM). Results are representative of one out of four independent experiments.

IC50sd (SS concentration necessary to decrease the spheroid diameter by 50%, µM) indicated in the associated table are mean±SD of four independent experiments with $^{\$}p<0.0001$ vs 24h.

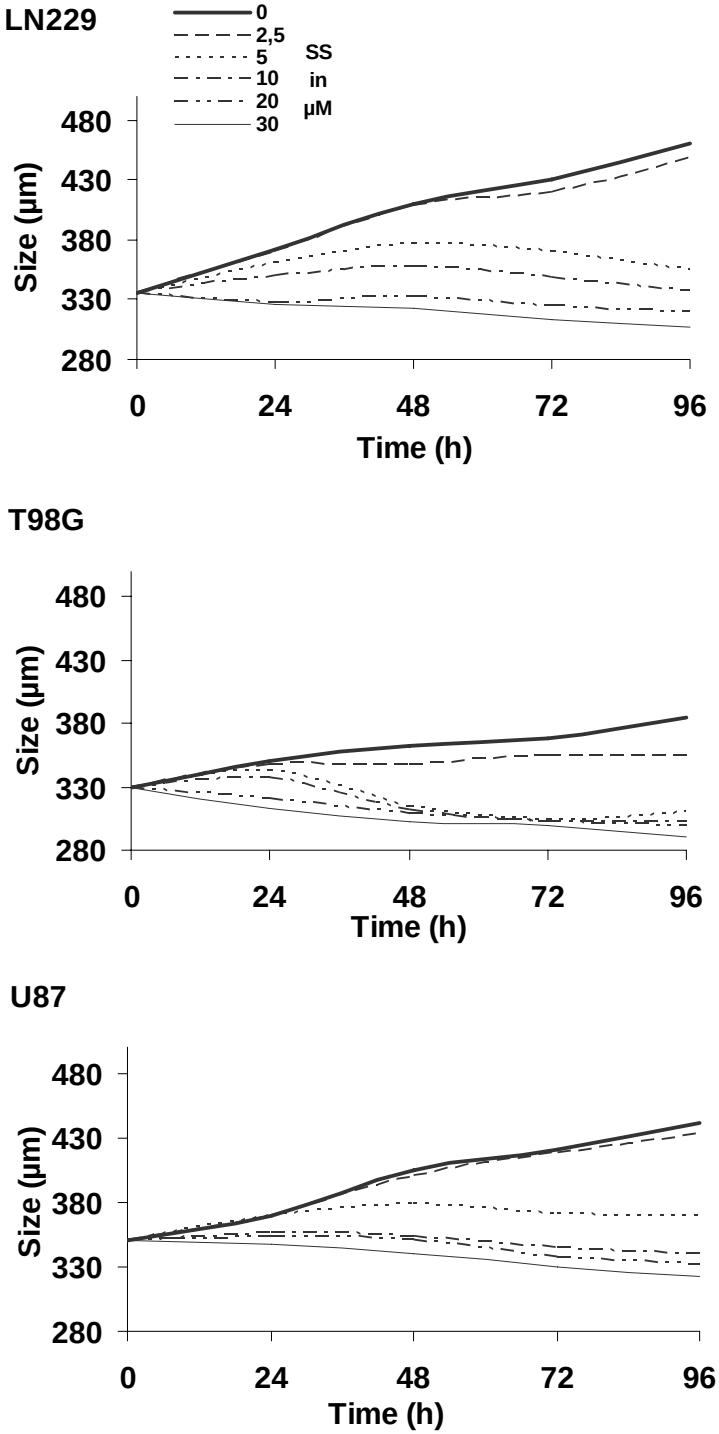

IC50sd (µM)	24h	48h	72h	96h
LN229	10.1±0.2	9.8±0.4	4.9±0.3$^{\$}$	4.5±0.2$^{\$}$
T98G	10.3±0.3	2.9±0.2$^{\$}$	3.1±0.1$^{\$}$	2.8±0.2$^{\$}$
U87	9.6±0.3	5.1±0.2$^{\$}$	4.8±0.1$^{\$}$	4.7±0.2$^{\$}$

Fig. 2B

Effects of sodium selenite on the cell cycle. Spheroids were prepared as described in the material and method section (3000 cells/well), cultured for 72h before the addition of SS. After 24h and 72h of SS treatment, spheroids were harvested, washed twice in PBS 1X then used for cell cycle determination by flow cytometry. Data expressed in percentage of positive cells, are mean±SD of three independent experiments and *p value* are indicated when significant versus control.

24h

	LN229	U87	T98G
Control	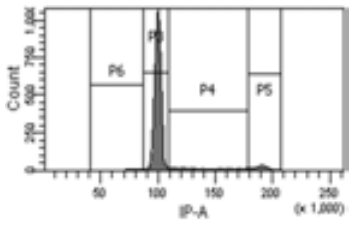	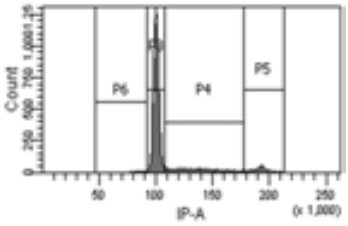	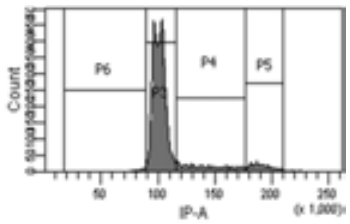
Sub G1 P6	0.8 ± 0.1	0.9 ± 0.4	0.4 ± 0.2
Go/G1 P3	77.6 ± 2.3	75.6 ± 4.0	74.7 ± 2.8
S P4	10.7 ± 1.0	14.2 ± 4.7	17.7 ± 1.5
G2/M P5	6.9 ± 0.8	5.1 ± 1.3	5.9 ± 1.2
SS 2.5µM	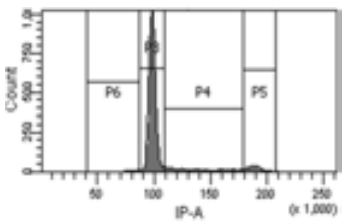	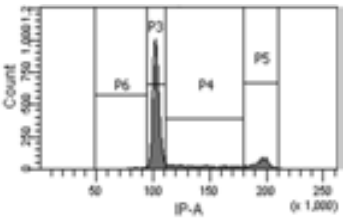	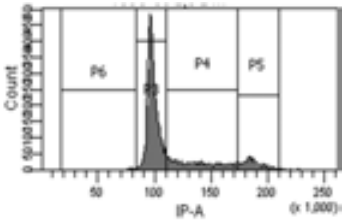
Sub G1 P6	0.7 ± 0.1	2.1 ± 1.5	0.5 ± 0.4
Go/G1 P3	77.2 ± 1.9	60.7 ± 11.6	60.9 ± 3.5 *p=0,01*
S P4	10.8 ± 0.8	24.4 ± 11.7	14.6 ± 1.1
G2/M P5	7.0 ± 0.9	9.2 ± 1.3	7.7 ± 0.3
SS 5µM	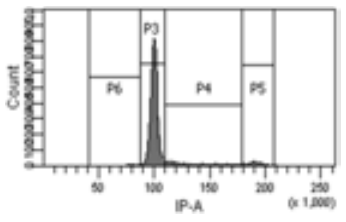	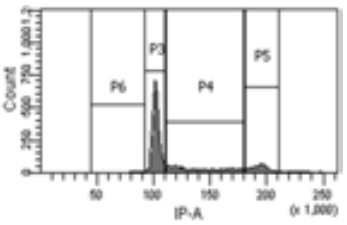	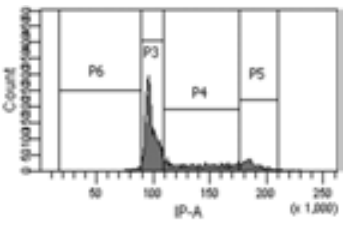
Sub G1 P6	0.9 ± 0.2	0.5 ± 0.1	1.1 ± 0.5
Go/G1 P3	75.9 ± 3.8	69.5 ± 5.9	61.8 ± 3.5 *p=0.01*
S P4	14.8 ± 2.5	19.9 ± 4.9	27.8 ± 2.9 *p=0.002*
G2/M P5	8.0 ± 1.2	8.9 ± 2.3	8.5 ± 1.1
SS 10µM	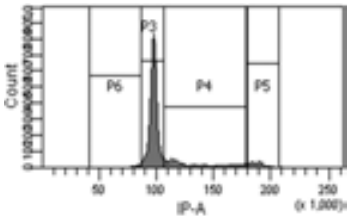	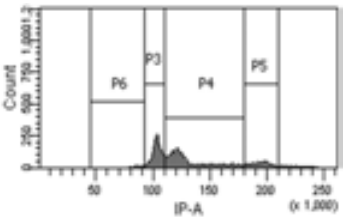	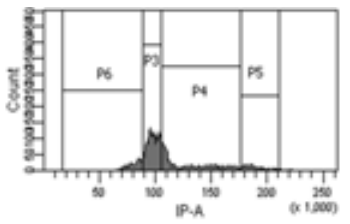
Sub G1 P6	1.1 ± 0.0	1.1 ± 0.3	5.9 ± 2.7 *p=0.02*
Go/G1 P3	72.4 ± 8.2	46.2 ± 14.4	47.4 ± 0.9 *p=0.002*
S P4	23.2 ± 4.0 *p=0. 004*	39.3 ± 14.3	38.0 ± 3,7 *p<0.0001*
G2/M P5	10.1 ± 1.6	9.4 ± 2.1	7.2 ± 0.9

Fig. 2B (followed…)

72h

		LN229	U87
Control		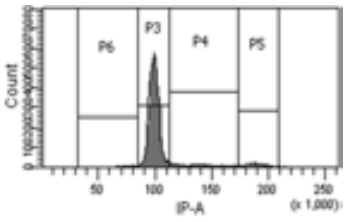	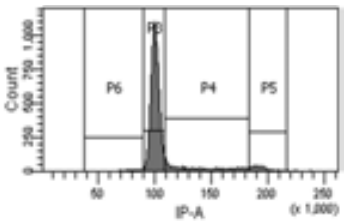
	Sub G1 P6	1.1 ± 0.2	0.5 ± 0.1
	Go/G1 P3	83.3 ± 2.2	83.3 ± 0.9
	S P4	9.4 ± 1.4	11.0 ± 0.8
	G2/M P5	5.9 ± 0.6	5.1 ± 0.5
SS 2.5µM		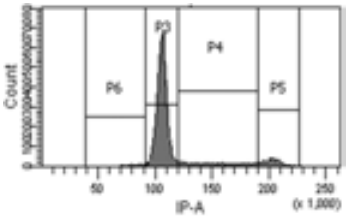	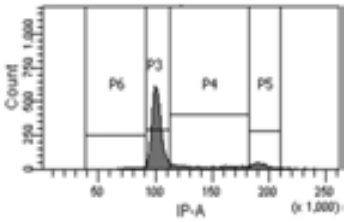
	Sub G1 P6	1.3 ± 0.1	1.1 ± 0.3
	Go/G1 P3	81.1 ± 0.6	75.6 ± 4.8
	S P4	10.6 ± 0.4	14.7 ± 3.5
	G2/M P5	6.9 ± 0.2	8.4 ± 1.0
SS 5µM		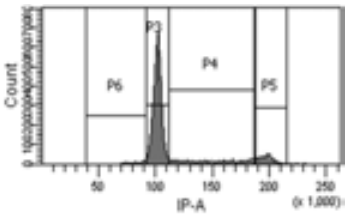	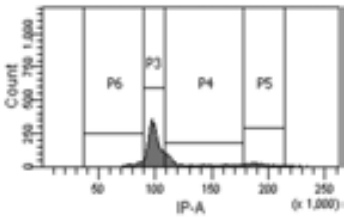
	Sub G1 P6	1.5 ± 0.3	4.5 ± 1.1 *p=0.02*
	Go/G1 P3	76.2 ± 0.5	52.5 ± 7.9 *p=0.007*
	S P4	12.7 ± 0.8	30.1 ± 6.6 *p=0.03*
	G2/M P5	9.4 ± 0.5	11.3 ± 1.4 *p=0.02*
SS 10µM		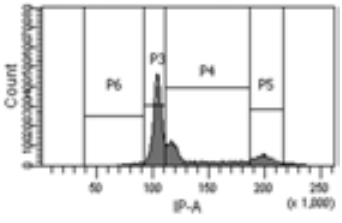	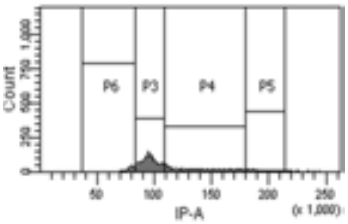
	Sub G1 P6	2.5 ± 0.6 *p=0.03*	6.8 ± 1.5 *p=0.002*
	Go/G1 P3	37.6 ± 7.8 *p<0.0001*	40.2 ± 7.8 *p=0.001*
	S P4	38.5 ± 4.7 *p<0.0001*	35.5 ± 6.4 *p=0.008*
	G2/M P5	18.0 ± 2.5 *p=0.0002*	10.1 ± 2.3 *p=0.03*

Figure 3. Anti invasiness properties of sodium selenite

Fig. 3A

Detachment and migration of cells from spheroids were followed after deposition of spheroids on Matrigel coated Petri-dishes. The size of spheroids was measured until 192h after the deposit.
Results are mean diameter (µm) ±SD of three independent experiments, with *p<0.05, **p<0.005 vs control at 24h.

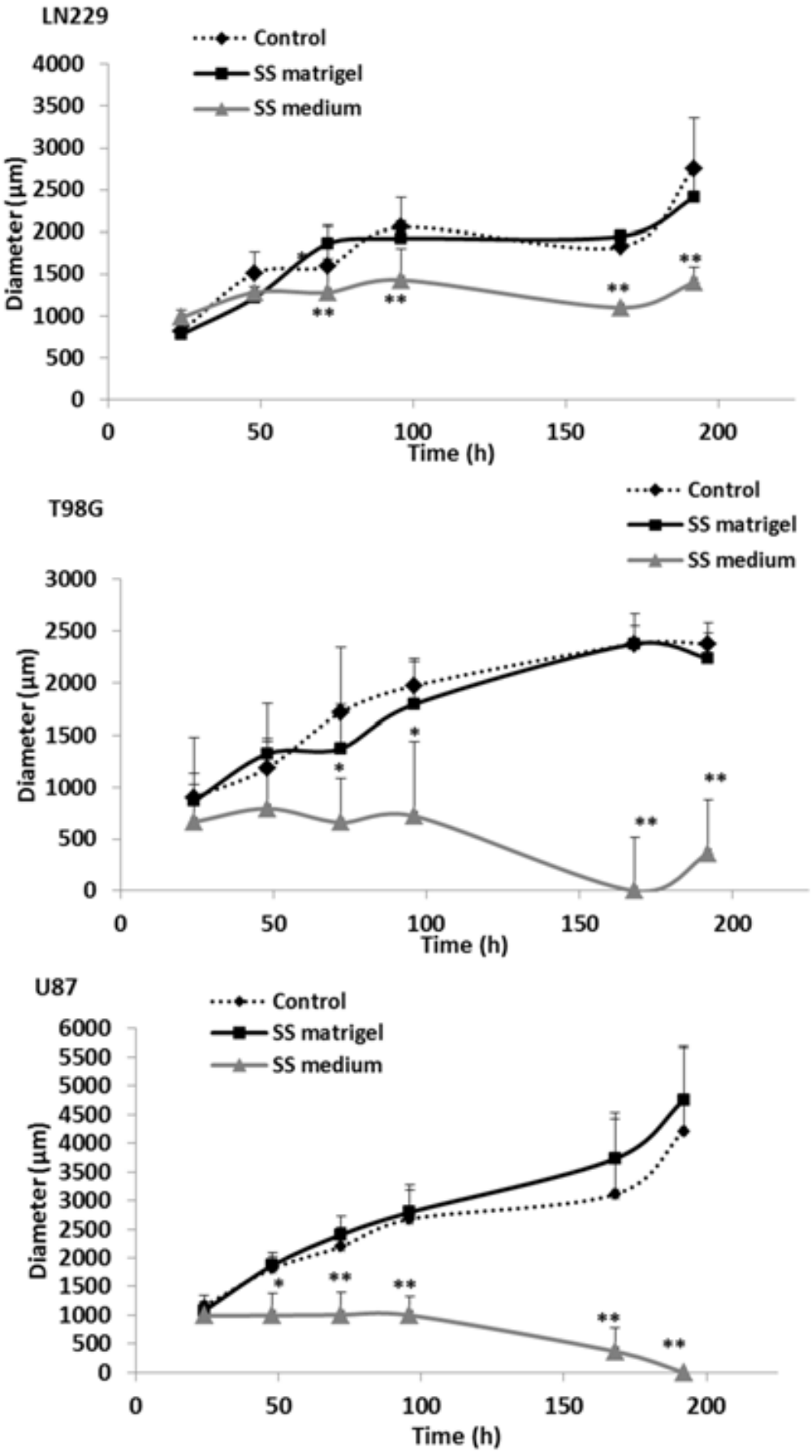

Fig. 3B

Pictures (X4) were taken after each measurement and are illustrative of three independent experiments.

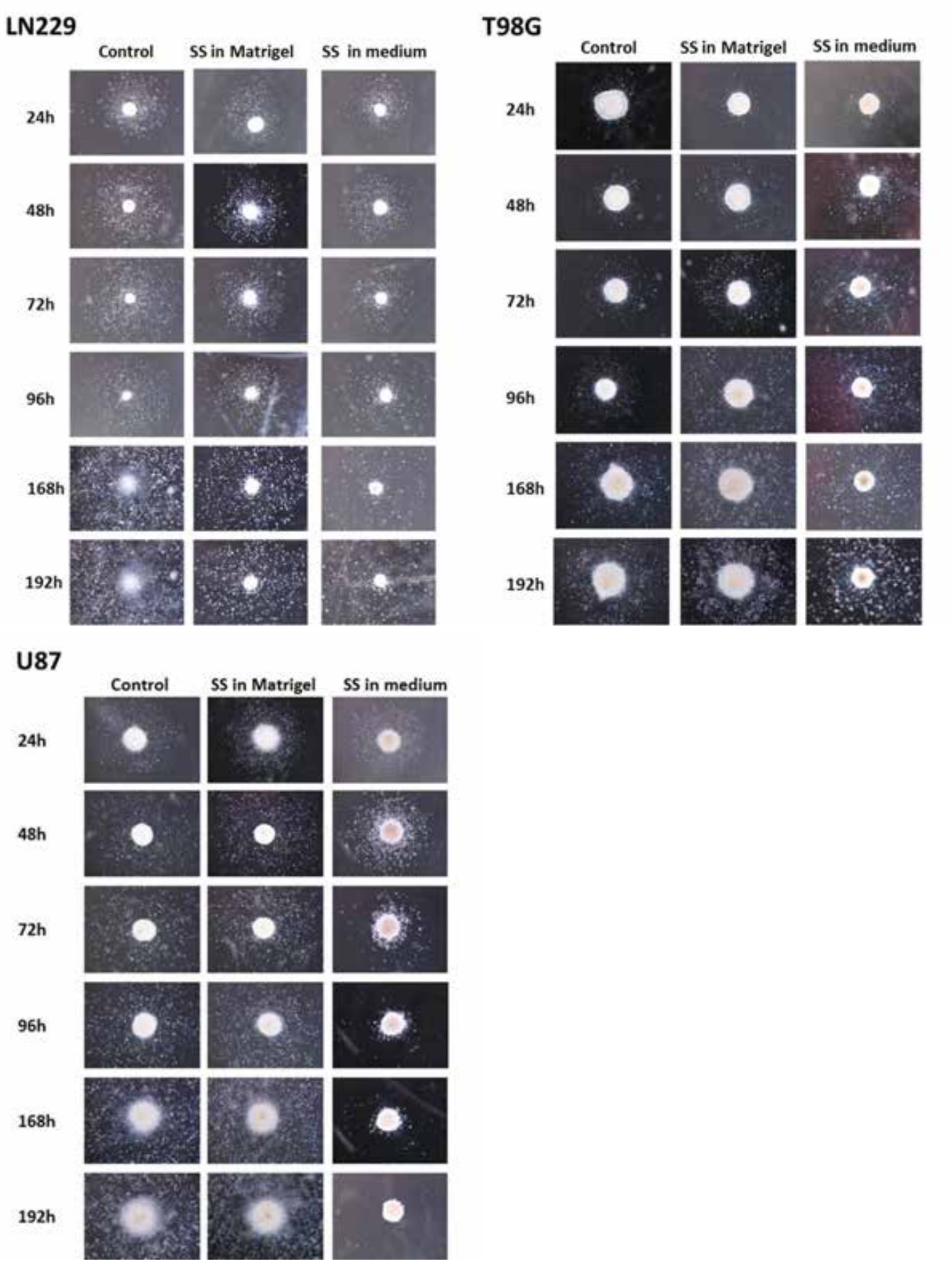

Fig. 3C

E-cadherin and N-cadherin transcript expressions were evaluated by RT-q-PCR. LN229, T98G and U87 in 3D were treated 72h with SS. Results are mean ±SD of three independent experiments, with $^{t}p=0.07$, *p<0.05, **p<0.005 vs control at 24h.

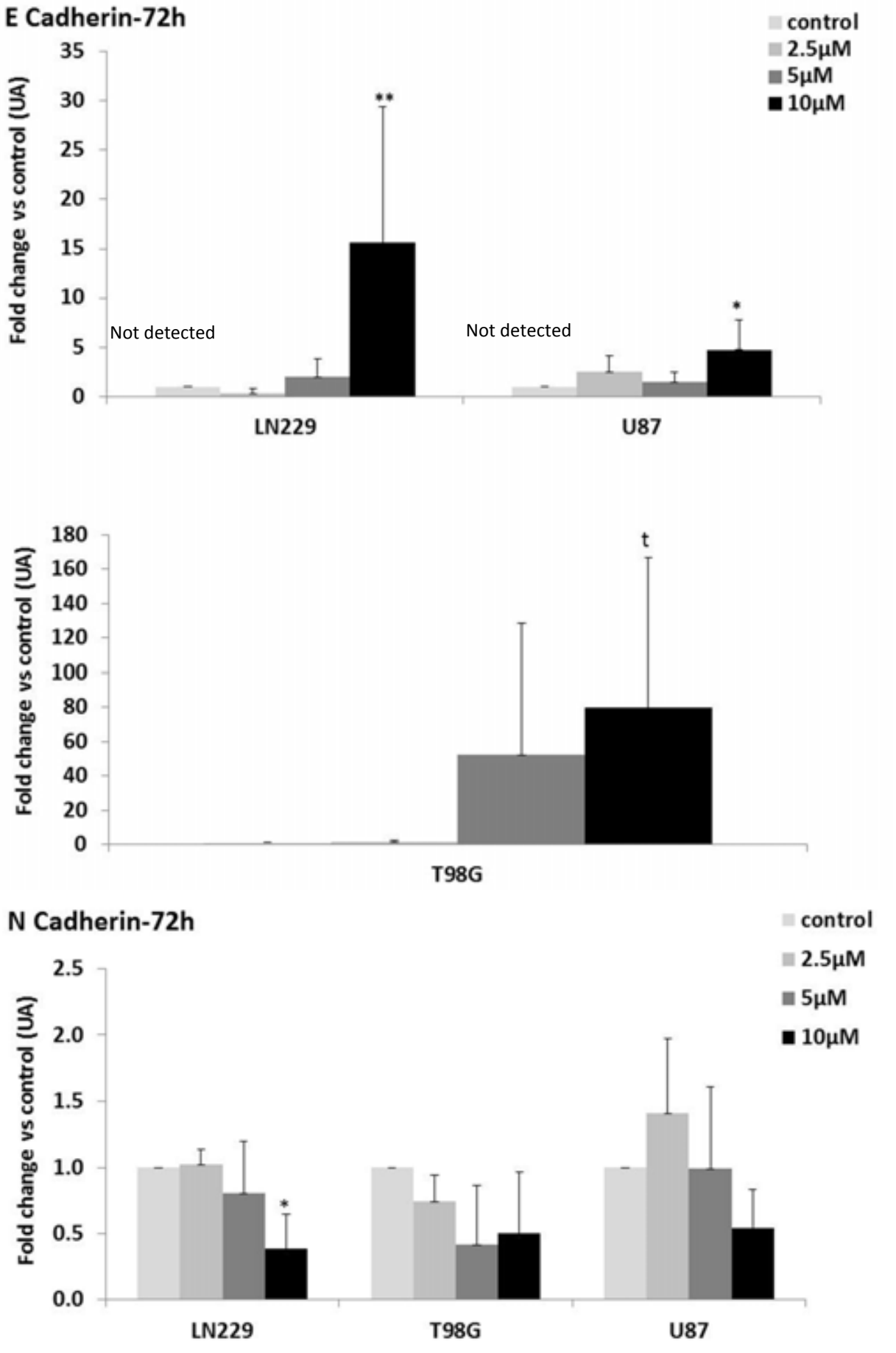

Figure 4. Sodium selenite decreased CA9 expression.
CA9 expression was evaluated both:

Fig. 4A

at the transcriptional level (real time PCR), 24h after SS treatment. Results are mean±SD of four independent experiments, expressed by fold change vs the control (not treated) with ***p<0.0005 and $p<0.001 vs control.

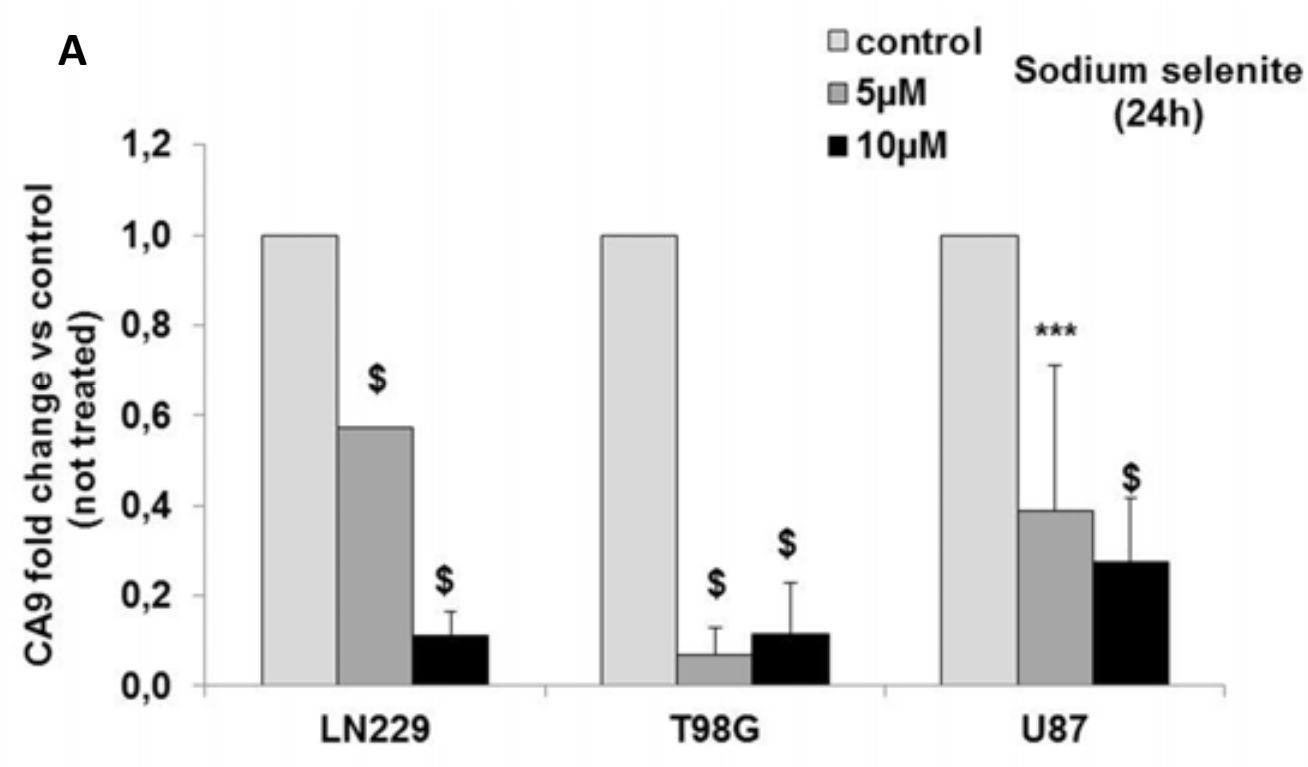

Fig. 4B

At the protein level, by immunohistochemistry. Pictures were performed at a magnification X400 and were representative of three independent experiments.

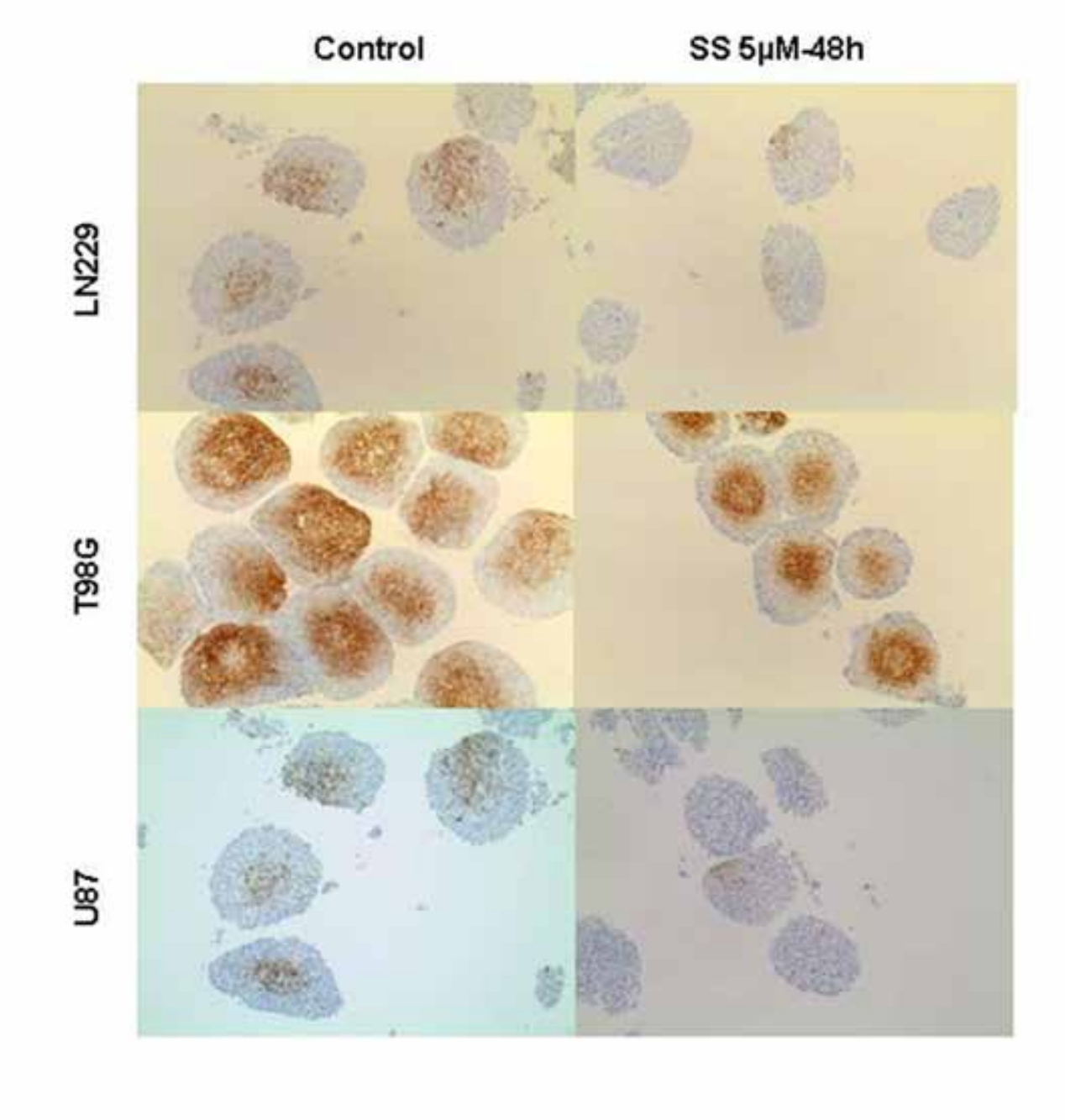

Figure 5. Sodium selenite is an epigenetic modulator.
HDAC activity was evaluated using a fluorometric method

Fig. 5A

lysates from LN229, T98G and U87 cells cultivated in 3D for 72h and treated 72h with SS at 2.5, 5µM and 10µM. Results expressed in Relative Fluorescence Units/µg of protein (% vs control) are mean±SD of three independent experiments with *p<0.05 and **p<0.005 versus the control (not treated cells).

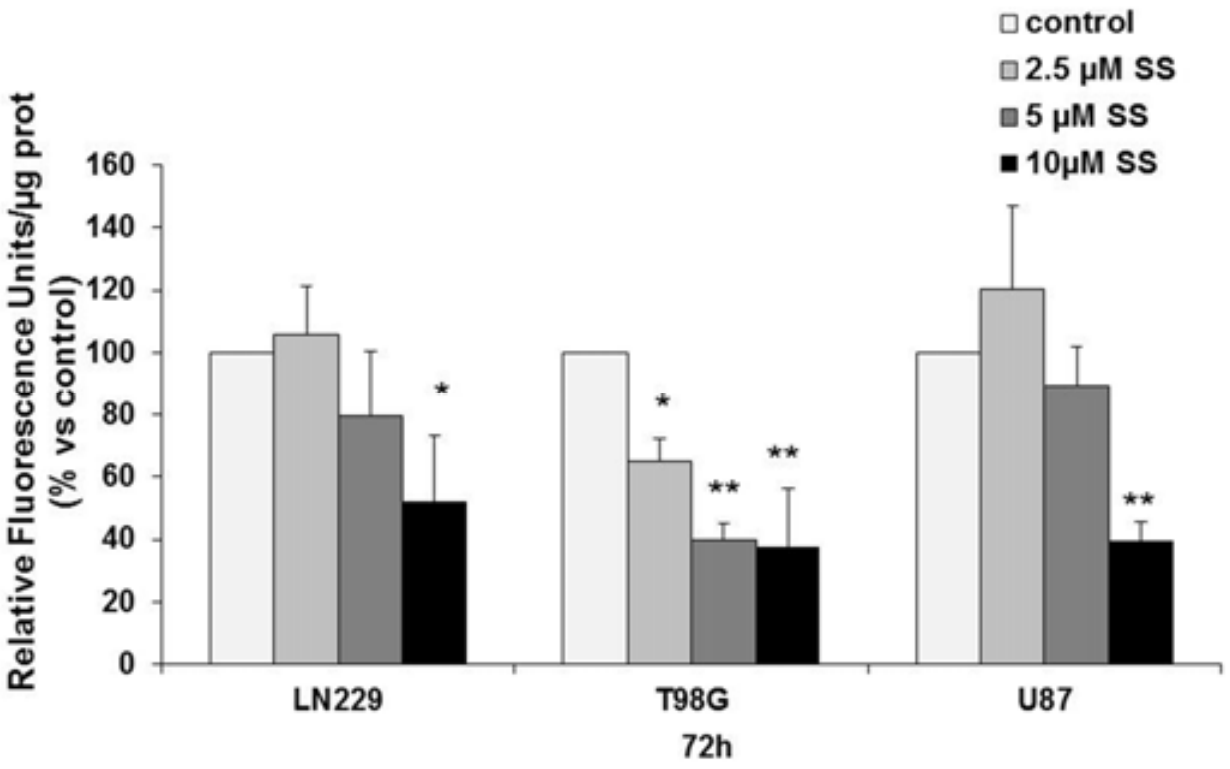

Fig. 5B

TSA or SS (both at 20µM) were directly added into the lysates and HDAC activity was determined. Results expressed in Relative Fluorescence Units/µg prot (% vs control) are mean±SD of three independent experiments with $p<0.0001 versus the control (not treated cells).

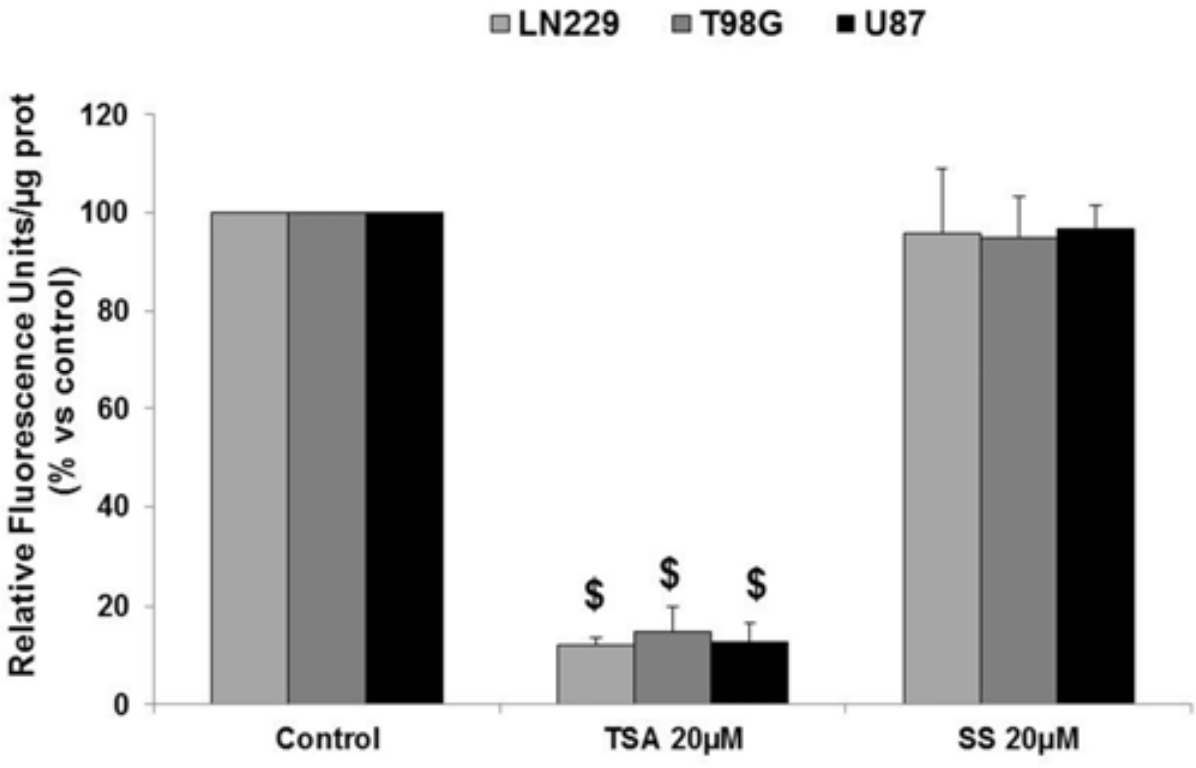

Fig. 5C Dimethyl H3K9 level was evaluated in LN229 and U87 cultivated in 3D. Spheroids were prepared as described, treated 24h with SS and dissociated with Accutase to be analyzed by flow cytometry. Left histograms represent the percentage of labelled cells versus non labelled cells and right histogram the mean fluorescence of labelled cells in P3. Results are mean±SD of three independent experiments with *p<0.05 and **p<0.005 versus the control (not treated cells).